

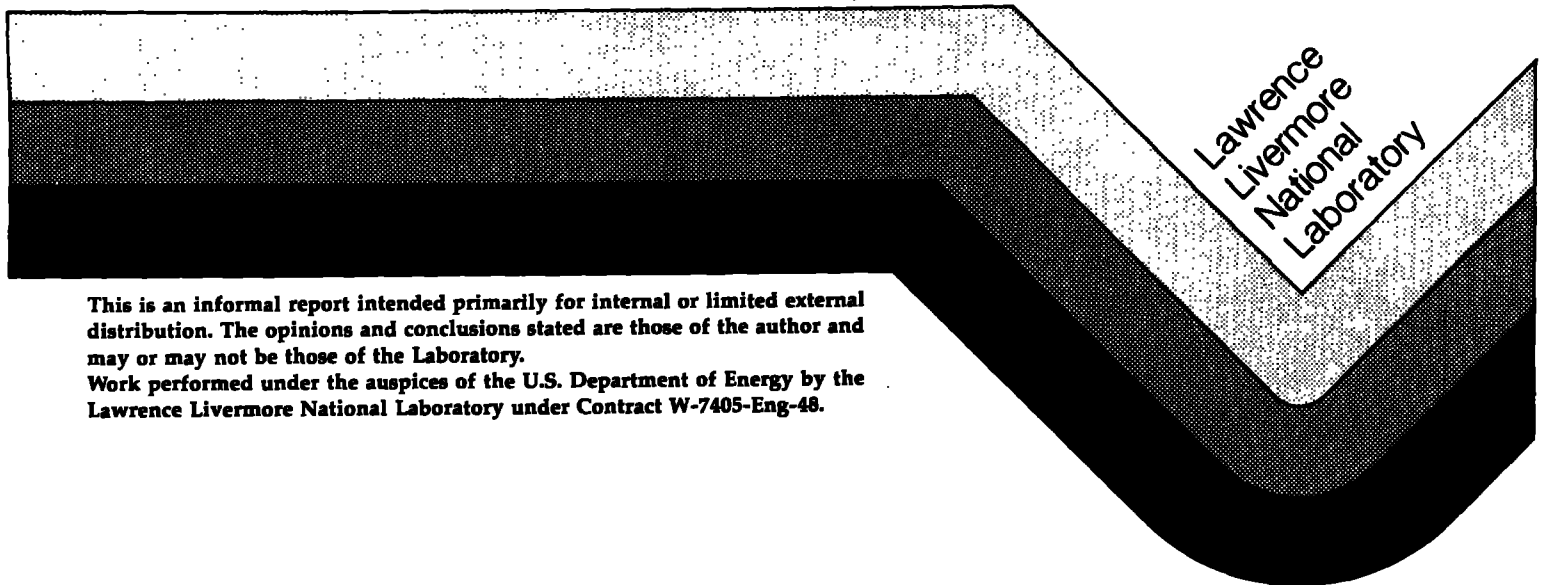
CIRCULAR COPY
SERIAL NO. 84-11
IN TWO VOLUMES

MATERIALS PHYSICS QUARTERLY REPORT

H DIVISION

April through June 1984

December 7, 1984



This is an informal report intended primarily for internal or limited external distribution. The opinions and conclusions stated are those of the author and may or may not be those of the Laboratory.

Work performed under the auspices of the U.S. Department of Energy by the Lawrence Livermore National Laboratory under Contract W-7405-Eng-48.

DISCLAIMER

This document was prepared as an account of work sponsored by an agency of the United States Government. Neither the United States Government nor the University of California nor any of their employees, makes any warranty, express or implied, or assumes any legal liability or responsibility for the accuracy, completeness, or usefulness of any information, apparatus, product, or process disclosed, or represents that its use would not infringe privately owned rights. Reference herein to any specific commercial products, process, or service by trade name, trademark, manufacturer, or otherwise, does not necessarily constitute or imply its endorsement, recommendation, or favoring by the United States Government or the University of California. The views and opinions of authors expressed herein do not necessarily state or reflect those of the United States Government or the University of California, and shall not be used for advertising or product endorsement purposes.

Printed in the United States of America
Available from
National Technical Information Service
U.S. Department of Commerce
5285 Port Royal Road
Springfield, VA 22161
Price: Printed Copy \$; Microfiche \$4.50

<u>Page Range</u>	<u>Domestic Price</u>	<u>Page Range</u>	<u>Domestic Price</u>
001-025	\$ 7.00	326-350	\$ 26.50
026-050	8.50	351-375	28.00
051-075	10.00	376-400	29.50
076-100	11.50	401-426	31.00
101-125	13.00	427-450	32.50
126-150	14.50	451-475	34.00
151-175	16.00	476-500	35.50
176-200	17.50	501-525	37.00
201-225	19.00	526-550	38.50
226-250	20.50	551-575	40.00
251-275	22.00	576-600	41.50
276-300	23.50	601-up ¹	
301-325	25.00		

¹Add 1.50 for each additional 25 page increment, or portion thereof from 601 pages up.

CONTENTS

HIGHLIGHTS.	1
---------------------	---

Experimental Physics

Railgun Development (R. S. Hawke and W. J. Nellis).	2
Ultrahigh-Pressure Underground Nuclear Driven Equation-of-State Experiment (A. C. Mitchell, W. J. Nellis, R. Olness, and J. K. Nash)	7
Equation-of-State of Nevada Tuff (B. Leroy Hord).	10

Static High Pressure Experiments

On the Possibility of Pr III Having a thcp Structure (G. S. Smith and J. Akella).	13
---	----

Condensed Matter Theory

Possible Missing Structure in the Rare-Earth Series (A. K. McMahan and D. A. Young).	18
Promotion Energies and Cohesion: A Simple, Accurate Scheme for Solids (J. A. Moriarty).	22
A General Correlation of Thermal Conductivity with Equation of State (R. Grover, W. Hoover, and W. Moran).	30

High Temperature Theory

Interdiffusion in a Dense, Binary Ionic Mixture (D. B. Boercker).	37
Oscillator Strengths Calculated from Effective Potentials (B. G. Wilson and F. J. Rogers)	43

Theoretical and Applied Mechanics

Compliant Material Response Characterization (A. C. Buckingham) . . .	50
Numerical Coupling of an Unstable Boundary Layer Flow and a Compliant Surface (M. S. Hall).	57
Three-Particle Heat Flow in One Dimension <u>via</u> the Boltzmann Equation (W. G. Hoover).	61

HIGHLIGHTS

- Solids are found in a wide variety of crystal structures and often undergo one or more structural phase transitions under conditions of increasing pressure and/or temperature. Microscopic understanding of the origins and trends in crystal phase stability has progressed to the point where meaningful predictions are sometimes possible. Recent experimental and theoretical work has uncovered a possible missing structure in the well-known rare-earth series. (See pp. 13 and 18.)
- Theoretical understanding of the transport properties of materials has lagged behind that of thermodynamic properties. A new analysis of computer simulation results suggest a direct correlation between the thermal conductivity of simple fluids and their excess entropy, allowing for tentative predictions of this quantity to about 10% accuracy. (See p. 29.) Other recent work related to transport properties is reported on pp. 37 and 61.

For comments or questions about this report, please contact the editor, John A. Moriarty (ext. 29964), or the individual authors.

EXPERIMENTAL PHYSICS

RAILGUN DEVELOPMENT

R. S. Hawke and W. J. Nellis

- Significant progress has been made toward the development of the railgun into a useful device for ultra-high pressure shockwave research. We have successfully and reliably operated a 1.6 m long railgun and 1 m long helium injector. Projectiles of 1 and 4 g mass were accelerated to 4.2 km/s and 3 km/s, respectively. We have solved the problems associated with gas and arc blowby, and vacuum operation. Agreement between code calculations and experiment were obtained for railgun performance and residual railgun deformation. Tests with a 5.2 m long railgun have commenced and to date 1 g has been accelerated to 4.8 km/s.

H-Division is developing the railgun into a useful device for ultra-high pressure shockwave research. The near term goal is to accelerate a 1 g projectile to 12 km/s (50% faster than the 2 stage light-gas gun). To reach this goal we designed, fabricated and tested a 1.6 m long prototype. The prototype operation was completely successful. We are now testing a 5 m long railgun.

Results of Tests with 1.6 m Prototype

The prototype system used a 1 m long 5000 psi helium gas injector to preaccelerate the projectile (1 g to 1.2 km/s and 4 g to 0.8 km/s). Preacceleration greatly reduces erosion of the railgun caused by the plasma arc armature. The railgun used Extrin for the insulator and copper for the rails. After assembly, the whole railgun and injector unit were precision bored, measured with an air gauge and inspected with a bore scope. The reaming technique produced bores with a diameter run-out less than 0.001" (25 μ m).

Strain gauges were mounted on the aluminum gas injector barrel and used to monitor the passage of the projectile. dB/dt probes were used to measure the passage of the magnetic field associated with the plasma arc armature and thereby provided diagnostics of the projectile travel in the railgun. Flash x-ray shadowgraphs were taken after projectile launch to determine velocity, projectile condition and tilt. Table I summarizes the major results of the

tests. The railgun operation was in good agreement with calculations made with our performance code (see Fig. 1). Figure 2 shows a copy of an x-ray shadowgraph of a 1 g projectile traveling at 4.2 km/s.

The railgun was operated at currents up to 350 kA, which in this launcher corresponds to an in-bore magnetic field intensity of about 6T and a propulsive pressure of 130 MPa (19,000 psi). Post operation inspection revealed that the bore in the region of peak current had a residual deformation of about 25 μm (0.001") which is in excellent agreement with Mike Chainyk's (NEED) NIKE 2D calculations. At the conclusion of the test series, we disassembled and sectioned the railgun barrel and found stress cracks in the insulator material. However, the cracks did not deter the railgun operation.

In summary, the 1.6 m railgun fully served its purpose and achieved the following milestones:

- Solved gas and arc blowby problems
- Reliable hard vacuum operation
- Controlled arc initiation
- Code/experiment agreement
 - Railgun performance
 - Residual railgun deformation

We are presently testing a 5 m long railgun and to date have accelerated 1 g to 4.8 km/s with a peak current of 220 kA.

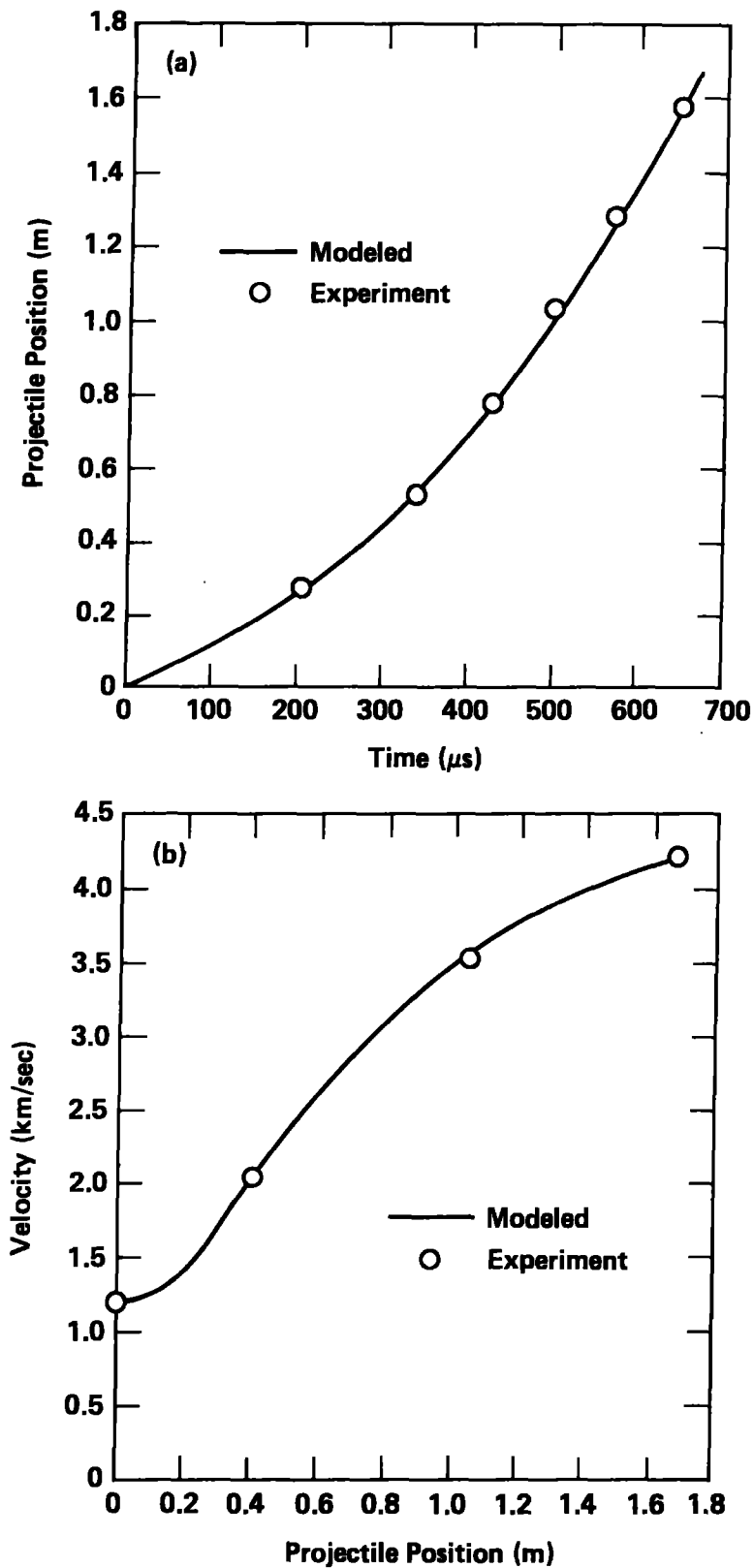


FIG. 1 Modeled and experimental performance for experiment 34, in which 1 g was accelerated to 4.2 km/sec: (a) shows the projectile position vs. time and (b) shows projectile velocity vs. projectile position.

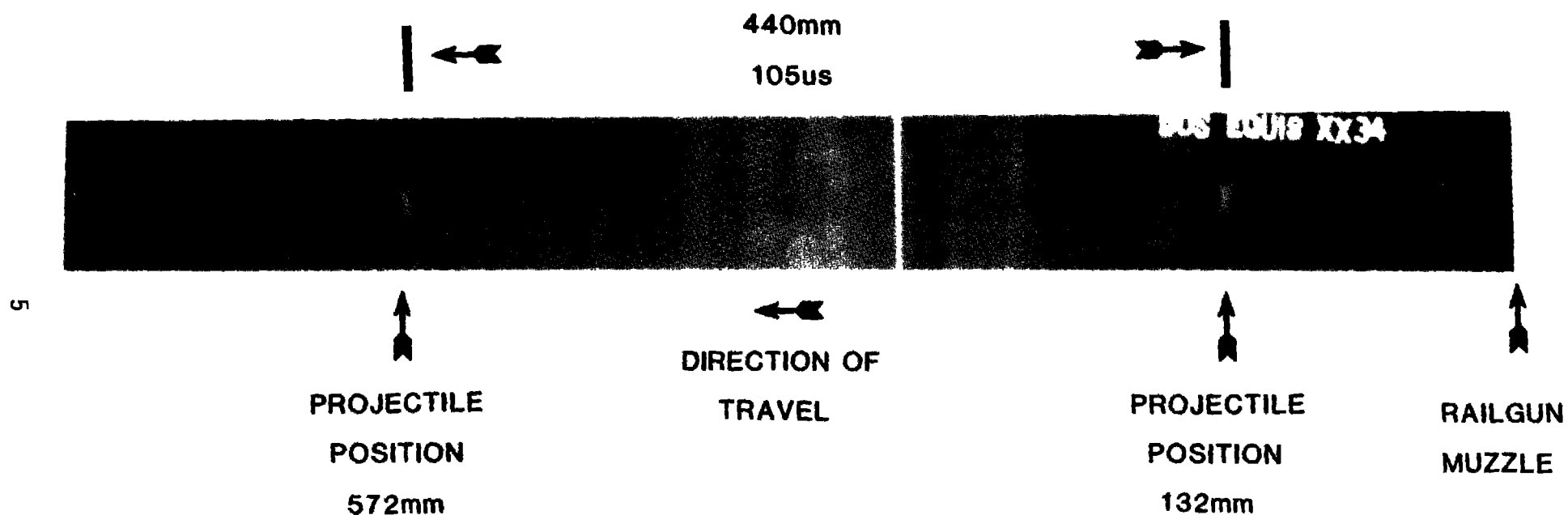


FIG. 2 Post launch double exposure x-ray shadowgraph of a 1 g projectile travelling 4.2 km/s. The projectile was completely intact and tilted less than 5 degrees in more than one half meter of post launch free flight.

TABLE I. Summary of major experimental results for the railgun tests.

<u>Experiment No.</u>	<u>29</u>	<u>31</u>	<u>32</u>	<u>33</u>	<u>34</u>	<u>40</u>	<u>41</u>
Projectile Mass (g)	1	1	1	1	1	4	4
Launch Velocity (km/s)	4.05	3.03	3.84	3.45	4.2	2.48	2.95
Initial Bank Energy (kJ)	103	106	106	110	103	160	230
Peak Current (kA)	225	220	225	225	220	300	350
Inductance Gradient ($\mu\text{H/m}$)	0.32	0.19	0.26	0.16	0.32	0.32	0.32
Δ Kinetic Energy (kJ)	7.9	3.9	6.5	4.4	8.2	20.7	15.9
Overall Efficiency (%)	7.7	3.7	6.1	4.0	7.9	6.7	6.9

ULTRAHIGH-PRESSURE UNDERGROUND NUCLEAR DRIVER EQUATION-OF-STATE EXPERIMENT

A. C. Mitchell, W. J. Nellis, R. Olness and J. K. Nash

- A pressure of 8.36 Mbar was obtained in aluminum from a nuclear-explosive-generated shock wave.

We have successfully fielded a shock impedance match experiment in close proximity to an underground nuclear explosion. This equation-of-state experiment was a joint effort between B Division (G. Repp) and L Division (R. Heinle). This experiment was similar to that described by the authors and C. Ragan.^{1,2,3} A planar shock wave was transmitted into a pure aluminum base plate, and shock impedance matched into samples which included carbon, copper and iron. In reference to the aluminum standard the shock pressures obtained in these materials are listed in Table I. In this experiment pure aluminum was chosen as the standard or reference material since its equation-of-state is known with some confidence.⁴ The statistical error in the measured shocked velocities ranged between 0.5 to 1.0% with the exception of carbon which was 1.5%. In all we had 96 shorting pins in and on the aluminum base and at various positions on specimens; all pins reported.

REFERENCES

1. A. C. Mitchell, W. J. Nellis, N. C. Holmes, M. Ross, G. W. Repp, R. A. Heinle, T. C. Valk, J. Rego, W. B. Graham, and R. J. Olness, "Shock Impedance Match Experiments in Aluminum and Molybdenum," in Shock Waves in Condensed Matter, North-Holland, New York, Ch. II:14, (1983), 81-83.
2. C. E. Ragan, "Ultrahigh-Pressure Shock Wave Experiments," Phys. Rev. A27 (1980), 458-463.
3. C. E. Ragan, et al., "Precise Ultrahigh-Pressure Experiments," in Shock Waves in Condensed Matter, North-Holland, New York, Ch. II:13 (1983), 77-80.
4. A. K. McMahan, "Isotherm and Hugoniot for Compressed Aluminum," Bull. Am. Phys. Soc. 21 (1976), 1303.

Table I. Pressures achieved in the present experiment.

<u>Material</u>	<u>Initial Density (gm/cc)</u>	<u>Pressure (Mbars)</u>
Al	2.698	8.36
C	2.203	7.64
Cu	8.934	14.7
Fe	7.869	14.1

EQUATION-OF-STATE OF NEVADA TUFF

B. Leroy Hord

- Shockwave equation-of-state measurements have been performed on a Nevada tuff rock specimen at .700 and .944 Mbars. The data points compare closely to earlier work on tuff of the same density.

The material properties of Nevada tuff have considerable variation from one location to another. It is therefore necessary to measure such properties on samples from each site of interest. Equation-of-state measurements were performed on tuff samples using the two-stage light-gas gun. The data were compared to previously measured samples from different sites.

Two impact shock wave measurements were made on dry tuff samples. Pressures obtained were .700 and .944 Mbars and fit within $\pm 3\%$ to high pressure data published by Shipman, Isbell and Jones.¹ Their curve of pressure vs. particle velocity is reproduced in Fig. 1 with the new points plotted as X's.

REFERENCE

1. Final report on High Pressure Hugoniot Measurements for Several Nevada Test Site Rocks, F. H. Shipman, W. M. Isbell, and A. H. Jones, March 1969, DASA-2214, MSL-68-15.

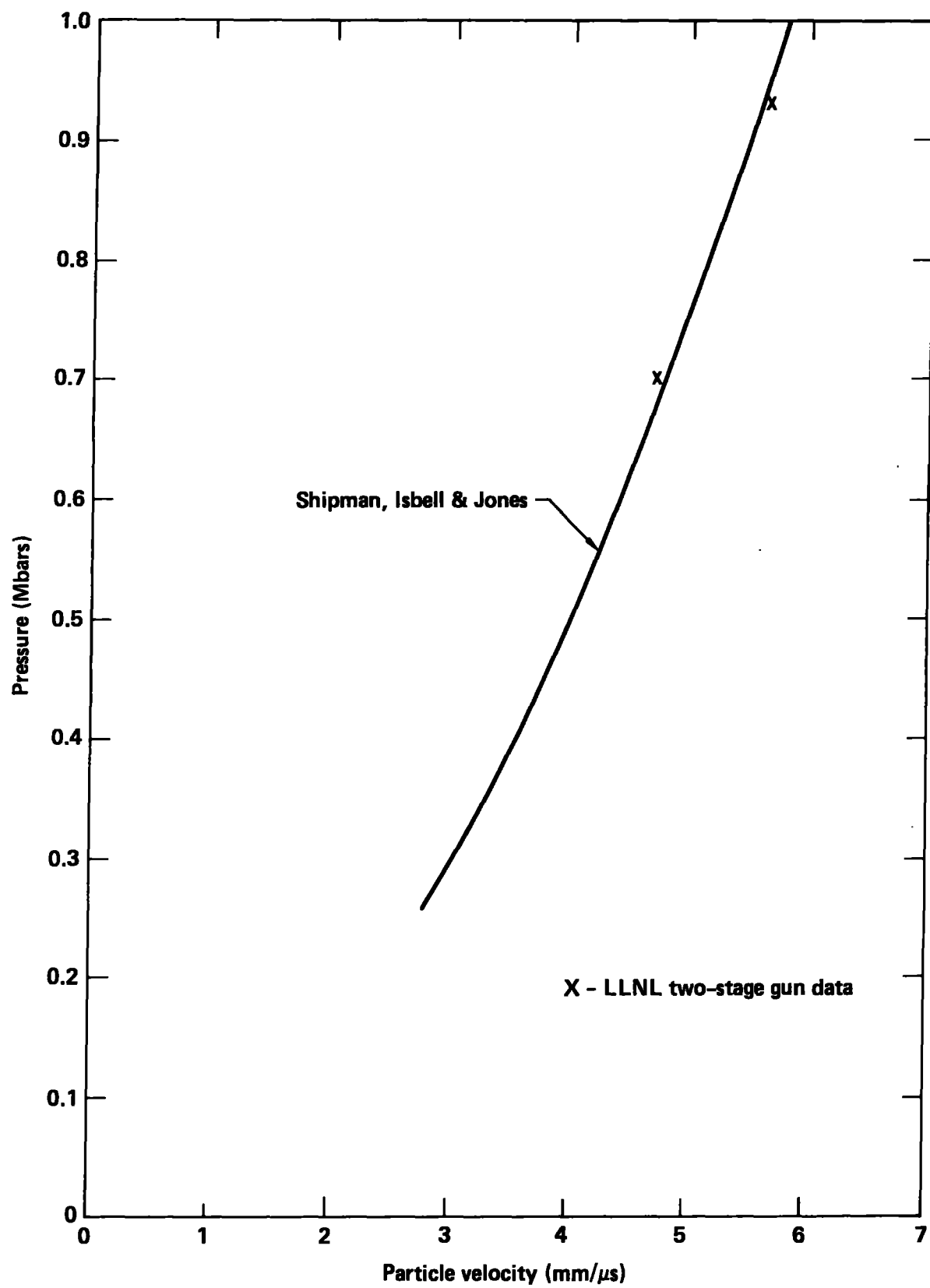


FIG. 1 Pressure vs. particle velocity in dry Nevada tuff.

STATIC HIGH PRESSURE EXPERIMENTS

ON THE POSSIBILITY OF Pr III HAVING A thcp STRUCTURE

Gordon S. Smith and Jagannadham Akella

- Crystallographic calculations have been carried out for a triple hexagonal close packed (=thcp) structure using data for Pr III, a high pressure form shown by praseodymium metal. McMahan and Young have proposed thcp as an additional high-pressure phase in the rare earth metals structural sequence. As applied to Pr III data at 14.4 GPa pressure, this structure-type accounts for most but not all of the diffraction lines. Thus, we are unable to establish conclusively that Pr III has a thcp structure. However, it is shown that the thcp structure fits the Pr III data as well as other structural forms proposed by other authors.

It is well known that the crystal structure changes in the lanthanide metals with increasing pressures are: hcp \rightarrow Sm-type \rightarrow dhcp \rightarrow fcc,¹ and these structures can be classified in terms of hexagonal-like and cubic-like layers. In these terms, the above sequence becomes: hhhhhh, hhchhc, chchch and cccccc. McMahan and Young² noted that, in this logical sequence, one structure-type was missing, namely cchcch. They referred to this six-layer crystal structure as "triple hexagonal close packed" (=thcp) by analogy with dhcp. In space group notation, the space group of a thcp structure is D_{6h}^4 - $P6_3/mmc$ with two atoms in 2b and four in 4f with $z = 1/12$. In terms of layers, A, B, C, thcp corresponds to ABCBAC.

We have examined the powder pattern of Mao, Hazen, Bell and Wittig³ for Pr III at 14.4 GPa (their Table 1) in terms of this newly proposed thcp structure. Least-squares refinement gives an hexagonal cell with $a = 3.220(5)$ Å and $c = 15.94(4)$ Å, $V = 143.2(4)$ Å³, $z = 6$ and $V/\text{atom} = 23.87(6)$ Å³. This atomic volume compares favorably with the value of 24.1 Å³ given by Mao, et al. for a larger orthorhombic cell that has almost twice the volume of the thcp cell. The c/a ratio of 4.951 is approximately 1% larger than the theoretical value of $\sqrt{24}$ (= 4.899) for a thcp structure.

Table I gives the comparison between observed and calculated d spacings and intensities.⁴ The thcp structure gives rise to several non space-group extinctions; for example, hhl lines for which $l = 6n$ are calculated to have zero for their structure factors. None of these lines were observed. Similarly, lines such as 100, 200, 106, 10 \cdot 12 etc. also have structure factors calculated to be zero. Likewise, none of these lines were observed either.

The agreement between observed and calculated d-spacings is fairly reasonable. Mao, et al.³ reported five additional lines which this thcp structure does not account for. It does not appear likely that these extra lines are remnant lines from the fcc Pr II phase. Three of these lines are observed at a minimal intensity of 10, and hence may be artifacts and not true lines of Pr III. The other two lines, $d = 2.87 \text{ \AA}$, $I = 30$ and $d = 1.549 \text{ \AA}$, $I = 40$ possibly could be MoK β lines of the $d = 2.624 \text{ \AA}$, $I = 100$ and $d = 1.374 \text{ \AA}$, $I = 70$ lines, respectively. It is to be noted that even the larger unit cell of Mao, et al. also does not account for the 2.87 \AA , $I = 30$ line.

As far as the agreement between observed and calculated intensities is concerned, all of the weak-to-strong lines permitted by the thcp structure are, with one exception, observed. The one exception is 203 with a calculated intensity of 17. On the other hand, two reflections calculated to be strong, 103 and 104, are observed to have intensities of 20 and 10, respectively.

In high pressure studies of Y, La, and Pr, Grosshans, Vohra and Holzapfel⁵ also reported powder patterns indexable on a hexagonal lattice with $c/a = \sqrt{24}$. They term this structure as a distorted fcc with a periodic distortion of the layer sequence ABCA'B'C' with increasing pressure. No experimental data were presented nor were atomic positions for their structural model given, and so we cannot compare the Grosshans, et al. distorted fcc structure with the present thcp type.

The theoretical calculations by McMahan and Young² show a small region of stability for a thcp structure between the dhcp and fcc phases. On the other hand, the interpretations of Grosshans, et al. and ourselves of experimental data suggest a six-layer structure after the disappearance of fcc. It should be noted that at still higher pressures Pr transforms into an α -uranium type structure, and this transformation is accompanied by a large volume decrease.⁶

In summary, the thcp structure accounts for some but not all of the diffraction data for Pr III. At this point, we do not claim thcp as firmly established, but we submit it as an interesting possibility. Clearly, further detailed experimental and theoretical studies of lanthanide series elements are required to confirm or deny this structure in the lanthanide sequence.

REFERENCES

1. A. Jayaraman, in Handbook of the Physics and Chemistry of the Rare Earths, ed. K. A. Gschneidner and L. Eyring, Vol. 1 (North-Holland, Amsterdam, 1978), Ch. 9.
2. A. K. McMahan and D. A. Young, Phys. Letters A (to be published). See also following report, p. 18.
3. H. K. Mao, R. M. Hazen, P. M. Bell and J. Wittig, J. Appl. Phys. 52, 4572 (1981).
4. Computer Programs Used: D. Appleman, Program and Abstracts, Amer. Cryst. Assoc. meeting, Cambridge, Mass. (1963) and D. K. Smith, Univ. of California report, UCRL-50264 (1967).
5. W. A. Grosshans, Y. K. Vohra and W. B. Holzapfel, Phys. Rev. Lett. 49, 1572 (1982).
6. G. S. Smith and J. Akella, J. Appl. Phys. 53, 9212 (1982).

Table I. Comparison of observed and calculated d spacings and intensities for Pr III at 14.4 GPa. Also given is $\Delta 2\theta = 2\theta_{\text{calc}} - 2\theta_{\text{obs}}$ for each line (λ assumed to be 0.7107 Å). Lines hkl for which l does not equal $6n$ are calculated to have zero intensities and are omitted.

$d_{\text{obs}}, \text{\AA}$	$d_{\text{calc}}, \text{\AA}$	hkl	$\Delta 2\theta$	I_{obs}	I_{calc}
--	2.789	100	--	--	0
2.768	2.747	101	+0.11	50	33
2.663	2.657	006	+0.03	60	59
2.624	2.633	102	-0.05	100	89
2.479	2.470	103	+0.06	20	100
2.282	2.285	104	-0.02	10	61
2.110	2.099	105	+0.10	20	16
--	1.924	106	--	--	0
1.754	1.764	107	-0.14	30	10
1.698	--	--	--	10	--
1.614	1.621	108	-0.12	40	22
	1.610	110	+0.06		45
1.549	--	--	--	40	--
1.497	1.495	109	+0.03	20	24
1.442	--	--	--	10	--
--	1.395	200	--	--	0
--	1.389	201	--	--	5
1.374	1.384	10•10	-0.23	70	14
	1.377	116	-0.07		54
	1.374	202	+0.01		14
--	1.349	203	--	--	17
1.311	1.316	204	-0.13	30	12
1.278	1.286	10•11	-0.21	20	4
	1.278	205	+0.01		4
1.232	1.235	206	-0.08	10	0
--	1.199	10•12	--	--	0
1.190	1.189	207	+0.02	10	3
1.144	1.143	208	+0.05	10	7

An additional line at $d = 2.87 \text{ \AA}$ with $I = 30$ is not indexed by the thcp unit cell nor by the larger orthorhombic cell of Mao, *et al.*³

POSSIBLE MISSING STRUCTURE IN THE RARE-EARTH SERIES

A. K. McMahan and D. A. Young

- It is suggested that the sequence of close-packed structures observed in the rare earths and heavier actinides is incomplete, and that closer investigation of individual members under pressure may well show an additional structure which might be called triple-hexagonal-close-packed (thcp).

It is well known that the trivalent rare-earth metals undergo the sequence of structural transitions: hexagonal-close packed (hcp) \rightarrow Sm-type (Sm) \rightarrow double-hexagonal-close packed (dhcp) \rightarrow face-centered cubic (fcc). These transitions occur for individual members under pressure, and across the series at zero pressure. The heavier actinides (beginning with Am) show the last part of this series in a similar manner. It is suggested here from a fundamental point of view that this sequence is incomplete, and that a fifth structure should be added to it.

The four rare-earth structures are among an infinite number of ways in which atoms can be close packed in a solid. Crystallographically, only for the hcp and fcc structures are all atoms within a given solid equivalent to one another. In all other cases there are two inequivalent sites, which by their local environment are naturally called hexagonal (h) and cubic (c), respectively. One can view all four rare-earth structures as a stacking of layers of atoms, where each layer is of a consistent type, i.e., either h or c. From this point of view the sequence is seen as a prolonged transition from hexagonal to cubic local symmetry: hhhhhh... (hcp) \rightarrow hhchhc... (Sm) \rightarrow hchchc... (dhcp) \rightarrow cccccc... (fcc). It is immediately obvious from this representation that the sequence itself lacks symmetry, in that a structure cchcch... is missing. Pauling¹ in fact mentioned such a structure, which is hexagonal with an axial ratio three times that of hcp, and which by analogy to

dhcp might thus be called triple-hexagonal-close packed. We are suggesting that it is thcp which should be added to complete the rare-earth sequence.

The physical mechanism for the sequence of transitions in the rare earths and late actinides is electronic s-d transition. Under pressure, or at zero pressure moving across the series, the relative positions of the 6s and 5d bands (rare earth case) are changing, with the result of an increase in the number of d electrons. The occupied s (actually sp hybrid) states lie close to the Brillouin zone center and are relatively insensitive to structure, while the f electrons in these materials are believed to be effectively inert. The changing structural energy differences thus come from the progressive filling of the 5d (6d) bands as individual rare earths (actinides) are compressed.

Figure 1 shows such energy differences calculated with Andersen's canonical d bands.² This is equivalent to the original work of Duthie and Pettifor³ explaining the rare-earth series, although now we have added the thcp phase. As can be seen, there is a very small range of stability for thcp for a d-band occupation between 2.57 and 2.65 electrons, positioned as to be expected between dhcp and fcc.

Since this work was originally carried out, Smith and Akella of LLNL have noted⁴ that thcp may be a candidate for the structure previously identified in high-pressure Pr as distorted fcc, although then the sequence would go dhcp → fcc → thcp, which is out of order with respect to the above discussion. The above canonical band calculations are rather approximate, however, and neglect the effects of hybridization. More rigorous LMT0 calculations for the high-pressure alkali metals show regions of the rare-earth structure sequence which are also out of order.

REFERENCES

1. L. Pauling, The Nature of the Chemical Bond, (Cornell Univ. Press, Ithaca, 1960).
2. O. K. Andersen, Phys. Rev. B 12, 3060 (1975).
3. J. C. Duthie and D. G. Pettifor, Phys. Rev. Lett. 38, 564 (1977).
4. See G. S. Smith and J. Akella, previous report, p. 13.

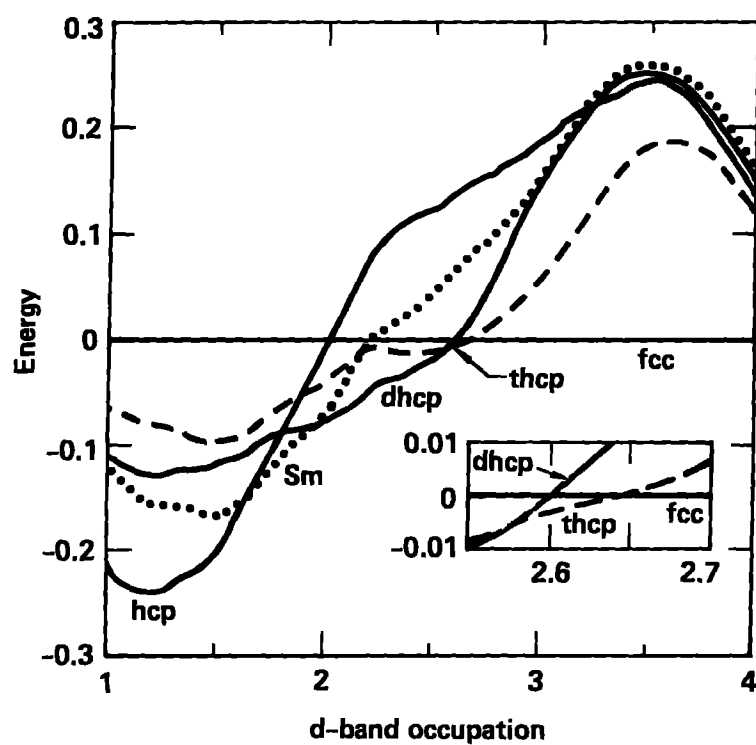


FIG. 1 Dimensionless energies for the five rare-earth structures as a function of d-band occupation. Energies are given relative to fcc. The small region of thcp stability is shown magnified in the insert.

PROMOTION ENERGIES AND COHESION: A SIMPLE, ACCURATE SCHEME FOR SOLIDS

J. A. Moriarty

- A simple, quantitatively reliable, formula has been derived for obtaining atomic promotion energies relevant to cohesion in solids. For the case of transition metals, this result has been combined with the generalized pseudopotential theory (GPT) to yield a simplified scheme for calculating accurate cohesive properties.

It is frequently the case that the ground-state electronic configuration of a solid differs from that of the corresponding free atom or atoms of which it is composed. This is true, for example, in tetrahedrally-coordinated semiconductors, where the $\underline{s} \rightarrow \underline{p}$ promotion of a valence electron is necessary to go from the $\underline{s}^2 \underline{p}^2$ free-atom configuration to an \underline{sp}^3 configuration from which directional hybrid orbitals and the covalent bond can be formed.¹ It is also true in transition metals, where hybridization typically induces either an $\underline{s} \rightarrow \underline{d}$ or $\underline{d} \rightarrow \underline{s}$ transfer of electrons as the metal is formed.^{2,3} In such cases, it is often convenient to introduce an atomic promotion energy associated with this electron transfer when discussing cohesion and the total energy of the solid.^{1,2} This concept, however, has heretofore not been systematically integrated with quantitative band-theory treatments of cohesion on semiconductors⁴ and transition metals⁵ based on the rigorous Kohn-Sham density-functional formalism.⁶ We report here on two advances in this direction. First, we have derived a very useful approximation formula for calculating the promotion energy in a general situation. Second, we have used this result to further develop a simplified, but accurate, approximation scheme for calculating the cohesive properties of transition metals in the context of the recently-extended generalized pseudopotential theory (GPT).^{3,7}

In transition metals, one envisages an electron promotion of the form

$$\begin{matrix} Z^0 & N-Z^0 \\ \underline{s} & \underline{s} \end{matrix} \underline{d} \text{ (free atom)} \rightarrow \begin{matrix} Z & N-Z \\ \underline{s} & \underline{s} \end{matrix} \underline{d} \text{ (metal)} , \quad (1)$$

with N an integer. The corresponding promotion energy is simply defined as

$$E_{\text{pro}} = E_{\text{tot}}^{\text{atom}}(Z_s) - E_{\text{tot}}^{\text{atom}}(Z_s^0), \quad (2)$$

where $E_{\text{tot}}^{\text{atom}}(Z_s)$ is the total energy of an atom with Z_s valence s electrons. Equation (2) may be readily evaluated within the framework of any self-consistent-field theory, but this usually provides no insight into the meaning of the result nor does it avoid the pitfall of subtracting two huge, nearly equal, numbers ($10^3 - 10^6$ Rydbergs in magnitude) to obtain a small number (on the order of 0.1 Rydbergs). A first approximation to E_{pro} which surmounts these difficulties is readily available in terms of the initial free-atom one-electron eigenvalues ϵ_i^0 and the occupation numbers α_i^0 and α_i^1 for the ground and excited states:

$$E_{\text{pro}}^0 = \sum_i (\alpha_i^1 - \alpha_i^0) \epsilon_i^0, \quad (3)$$

where the sum is over all orbitals i . Only the orbitals spanned by the promoted electron(s) give nonzero contributions on the right-hand-side of Eq. (3), so the net result is normally quite simple. The accuracy of Eq. (3) depends on the extent to which the electron density of the excited-state configuration, say n_1 , differs from that of the ground state, say n_0 . In the context of the Kohn-Sham local density formalism,⁶ where the total energy is written as a functional of the electron density, we have shown that Eq. (3) is correct to first-order in $\delta n = n_1 - n_0$. Unfortunately, in transition metals, where the relevant s and d orbitals differ greatly and relaxation effects are important, this result is too crude to be of practical use. Nonetheless, if one formally proceeds with a perturbation expansion in powers of δn , a useful result can be obtained. We have shown that to second-order in δn , one obtains the average promotion energy formula

$$\bar{E}_{\text{pro}} = \frac{1}{2} \sum_i (\alpha_i^1 - \alpha_i^0) (\epsilon_i^1 + \epsilon_i^0), \quad (4)$$

with ϵ_i^1 the corresponding excited-state eigenvalue for orbital i . Moreover, this latter result is exact with respect to all direct Coulomb terms and the

leading correction, of order $(\delta n)^3$, involves only exchange and correlation terms. This makes Eq. (4) reliable even when ϵ_i^1 and ϵ_i^0 differ significantly, as is the case in transition metals (See Fig. 1).

For the 3d transition series of elements, Eqs. (3) and (4) reduce to the simple expressions

$$E_{\text{pro}}^0 = (Z_s - Z_s^0) (\epsilon_{4s}^0 - \epsilon_{3d}^0) \quad (5)$$

and

$$\bar{E}_{\text{pro}} = \frac{1}{2} (Z_s - Z_s^0) [(\epsilon_{4s}^1 - \epsilon_{3d}^1) + (\epsilon_{4s}^0 - \epsilon_{3d}^0)] , \quad (6)$$

respectively. The respective quantitative accuracies of Eqs. (5) and (6) are contrasted in Table I as a function of $Z_s - Z_s^0$ (which in the GPT is an implicit function of volume). It can be seen that E_{pro}^0 underestimates the exact promotion energy obtained from Eq. (2) by up to 70%, whereas Eq. (6) for \bar{E}_{pro} is accurate to within 5% even for the worse case where $Z_s - Z_s^0 > 1$. Moreover, the error in the latter case is systematic and a smooth function of volume, so that the actual error incurred in volume derivatives of E_{pro} is significantly smaller, making the result useful for quantitative calculations of cohesion.

In the context of the transition-metal GPT, one can now view the formation of the metal in a three-step process, as illustrated in Fig. 1 for copper. First, one allows the appropriate s \rightarrow d atomic transfer of electrons. Because this transfer shifts well localized d electrons to less localized s orbitals, both the s and d one-electron levels fall in energy, even though $E_{\text{pro}} > 0$. Next, one permits the s electron density to be spread out uniformly at a density Z_s/Ω appropriate to the metal. This transfers electrons from outside an atomic volume Ω to within, pushing the d level higher in energy and generally above its original position in the free atom. Both the electron density and the position E_d and occupation Z_d of the d states in this pseudoatom then closely approximate the actual metal. The final step is to allow the broadening of full energy bands in the solid.

To utilize the promotion energy concept in total energy calculations, one can write the cohesive energy of the metal directly in terms of E_{pro} :

$$\begin{aligned} E_{\text{coh}} &= E_{\text{tot}}^{\text{metal}}(Z_s) - E_{\text{tot}}^{\text{atom}}(Z_s^0) \\ &= E_{\text{tot}}^{\text{metal}}(Z_s) - E_{\text{tot}}^{\text{atom}}(Z_s) + E_{\text{pro}} . \end{aligned} \quad (7)$$

The second form of Eq. (7) allows one to make a greatly simplifying analytic cancellation of the huge core energies inherent in the first two terms, so that E_{coh} can be calculated as a difference between the much smaller valence binding energies of the Z_s valence electrons.⁸ Replacing E_{pro} with \bar{E}_{pro} , one finally has

$$E_{\text{coh}} = E_{\text{bind}}^{\text{metal}}(Z_s) - E_{\text{bind}}^{\text{atom}}(Z_s) + \bar{E}_{\text{pro}} . \quad (8)$$

The quantitative accuracy of Eq. (8) for the case of copper is demonstrated in Table II, where it is shown that the calculated values of the cohesive energy, equilibrium atomic volume, and bulk modulus rival those of muffin-tin band theory based on full total-energy calculations.

REFERENCES

1. W. A. Harrison, Electronic Structure and the Properties of Solids, (Freeman, San Francisco, 1979).
2. C. D. Gelatt, Jr., H. Ehrenreich, and R. E. Watson, Phys. Rev. B 15, 1613 (1977).
3. J. A. Moriarty, Phys. Rev. B 26, 1754 (1982).
4. e.g., M. T. Yin and M. L. Cohen, Phys. Rev. B 26, 5668 (1982).
5. V. L. Moruzzi, J. F. Janak, and A. R. Williams, Calculated Electronic Properties of Metals (Pergamon, New York, 1978).
6. W. Kohn and L. J. Sham, Phys. Rev. 140, A1133 (1965).
7. J. A. Moriarty, UCID-18574-83-4, p. 14.
8. J. A. Moriarty, Phys. Rev. B 19, 609 (1979).

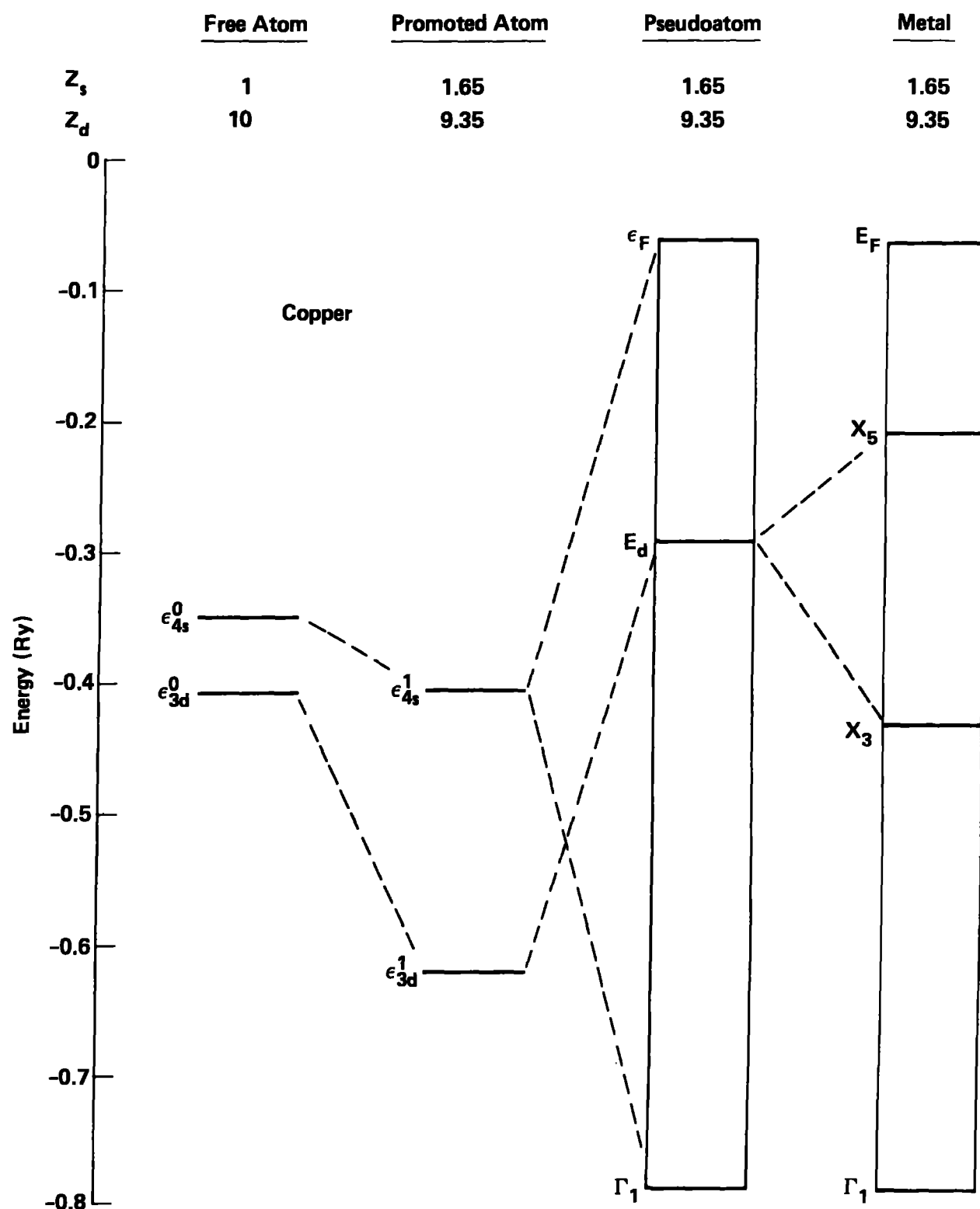


FIG. 1 Evolution of the valence energy levels from the free atom to the metal in copper. Energies and noninteger s and d occupation values, Z_s and Z_d , refer to the equilibrium atomic volume $\Omega_0 = 79.68$ a.u. in the metal.

Table I. Promotion energies for copper as a function of atomic volume Ω , as obtained from the approximation formulas, Eqs. (5) and (6), and exactly from Eq. (2) via total-energy subtraction. Here $Z_0^0 = 1$, Ω is in a.u., and all energies are given in Ry.

Ω	$Z_s - Z_s^0$	E_{pro}^0	\bar{E}_{pro}	$E_{\text{pro}}(\text{exact})$
107.64	0.469	0.027	0.053	0.052
93.66	0.553	0.032	0.068	0.067
79.68	0.654	0.038	0.089	0.087
65.70	0.776	0.045	0.119	0.115
51.72	0.924	0.054	0.161	0.155
37.74	1.100	0.065	0.221	0.211

Table II. Zero-temperature cohesive energy (E_{coh}), equilibrium atomic volume (Ω_0), and bulk modulus (B) for copper, as calculated from the generalized pseudopotential theory (GPT) via Eqs. (6) and (8) and muffin-tin band theory via total-energy subtraction (Ref. 5) and compared with experiment.

	GPT	Band Theory	Experiment
E_{coh} (Ry)	0.243	0.301	0.257
Ω_0 (a.u.)	76.5	77.5	78.9
$B(\Omega_0)$ (Mbar)	1.66	1.55	1.42

A GENERAL CORRELATION OF THERMAL CONDUCTIVITY WITH EQUATION OF STATE

R. Grover, W. Hoover, and W. Moran

- The (non-electronic) thermal conductivity K of a simple mon-atomic liquid appears to be an approximately universal function of its excess entropy at lower temperatures. This relation, deduced from many-body computer simulations, now allows one to estimate K for a simple fluid at high pressures from its equation-of-state to about 10% accuracy.

At present much less is known experimentally about the transport properties of fluids at high pressures than about their equation-of-state (EOS). In spite of extensive past study, transport theory is also less complete for fluids than EOS theory. We have used recent more extensive molecular dynamic calculations of the transport properties of many body systems with simple interaction pair potentials¹ to explore systematically the connection with equation-of-state properties. Close (but unspecified) connections are expected to exist according to the Chapman-Enskog theory for fluid transport properties, based on hard sphere interactions, since it is hard-sphere interactions, through a variational-perturbation theory (VPT), which provides a successful representation of the equation-of-state of simple liquids.²

Advances in non-equilibrium molecular dynamic simulation techniques³ have permitted the efficient study of transport in many particle systems in both high and low gradients and as a function of the interaction pair potential. Thermal conductivity calculations for a variety of inverse n -power potentials (including more recent results for $n=6$) and the Lennard-Jones pair potentials⁴ are now available for 108 particle systems as well as reliable equations-of-state from previous computer simulations by the Monte Carlo method. The extensiveness of this data base as well as some theoretical considerations suggest that the observed correlations between transport properties and EOS are generally valid.

The observed correlation is between two experimentally determined quantities: a reduced, dimensionless conductivity, K_R , expressed in terms of atomic and EOS parameters⁵, and a dimensionless deficit entropy, s , defined by

$$K_R \equiv \frac{M^{1/2}}{k_B^{3/2}} \frac{K}{\rho^{2/3} T^{1/2}} \quad (1)$$

$$s \equiv -S_x/k_B$$

in terms of the Boltzmann constant k_B , atomic mass M , particle number density ρ , temperature T and excess entropy (per atom) S_x . The appropriateness of the excess entropy in understanding EOS properties of fluids was pointed out by Rosenfeld⁶ as a simple consequence of the accuracy of VPT's of EOS such as Ross's.² The excess entropy in these theories is that of a hard-sphere system with a packing fraction which optimizes the model free energy.

It is, therefore, natural to explore the applicability of Chapman-Enskog hardsphere models to the various simulated systems by comparing their reduced transport coefficients as a function of deficit entropy. When Rosenfeld first did this for reduced viscosity and self-diffusion coefficients⁷ as functions of deficit entropy, he found only a rough similarity in the s dependence among the different pair potentials. In Fig. 1 the results of analytic conductivity fits to extensive hard-sphere⁸ ($n = \infty$) and soft-sphere ($n = 12$) calculations¹ are compared with the relatively few calculations available for the OCP ($n = 1$) and $n = 6$ systems. It is seen that to 10% and within accuracy of the individual points shown, the deficit entropy dependence of the reduced conductivity is the same for all inverse-power systems, in contrast to the situation for reduced viscosities. The comparisons in Fig. 1 correspond to a large but limited range of lower fluid temperatures ($< \sim 20$ melting temperature) where the results are of most interest.

The invariance of the s dependence of reduced conductivities shown in Fig. 1 suggests the same invariance for all pair potentials. This turned out to be the case for EOS because of additivity properties satisfied by hard-

sphere VPT for additive pair potentials. This property arises from the similarity of the fluid structure factors of all fluids regardless of pair potentials. To the extent that thermal conductivity involves convolution of the pair potentials (or its derivatives) with functions derived from fluid pair distribution functions we may expect similar additivity properties for transport coefficients. This in turn implies that K_R will have the same s dependence for a very general class of pair potentials.

This suggestion is supported by Fig. 2 where we show reduced conductivity vs. deficit entropy for 108 particle systems with the Lennard-Jones potential⁴ (which is a linear combination of inverse 12 and 6 power potentials), evaluated from data obtained by somewhat older molecular dynamic techniques. The points shown arise from two separate isotherms, and loci of points along the freezing line at high density and the saturated liquid-vapor line at lower densities. One recent highly accurate point by Evans⁹ at the triple point is also shown. These L-J points cover a wide range of densities where the Grüneisen γ of the solid phase is rapidly varying between 2 to 4. All points are in close agreement with the deficit entropy dependence of K_R for inverse- n -potential.

In addition to permitting a useful estimate of thermal conductivity of a fluid from its EOS, these results are theoretically interesting in showing that a close representation of liquid thermal conductivities by Enskog theory can be obtained with the use of hard-sphere conductivities and optimized hard-sphere packing fractions, $\xi(\rho, T)$, from hard-sphere VPT for EOS. The advantages of this method of determining $\xi(\rho, T)$ over other methods is illustrated in Fig. 3, where the results for several commonly used methods are compared for soft-sphere interactions. Values of ξ determined from soft-sphere thermal total pressures, $(\partial P / \partial T)_V$ (another measure of thermal pressures) and viscosity, via computer simulations for the hard-sphere system, are seen to differ significantly from those determined by VPT (and thermal conductivity).

REFERENCES

1. $n = \infty$: B. J. Alder, D. M. Gass and T. E. Wainright, J. Chem. Phys. 53, 3813 (1970).
 - 1: B. Bernu and P. Viellefoss, Phys. Rev. 18, 2345 (1978).
 - 12: W. T. Ashurst, Ph.D. Dissertation (Univ. Cal., Davis, 1974).
W. G. Hoover, B. Moran and J. M. Haile (to be published).
2. M. Ross, J. Chem. Phys. 71, 1567 (1979).
3. See articles in Physics Today 37 (January, 1984).
4. W. T. Ashurst - see Ref. (1).
5. Note that transport coefficients calculated for specific potentials are often scaled to the parameters in the pair potential, which is, however, unknown for real liquids. Definition (1) is thus a more convenient reduction for empirical applications.
6. Y. Rosenfeld, Phys. Rev. A 26, 3633 (1982) and A 28, 3063 (1983).
7. Y. Rosenfeld, Phys. Rev. A 15, 2545 (1977).
8. J. H. Dymond, J. Chem. Phys. 60, 969 (1974).
9. D. J. Evans, Phys. Lett. 91A, 457 (1982).

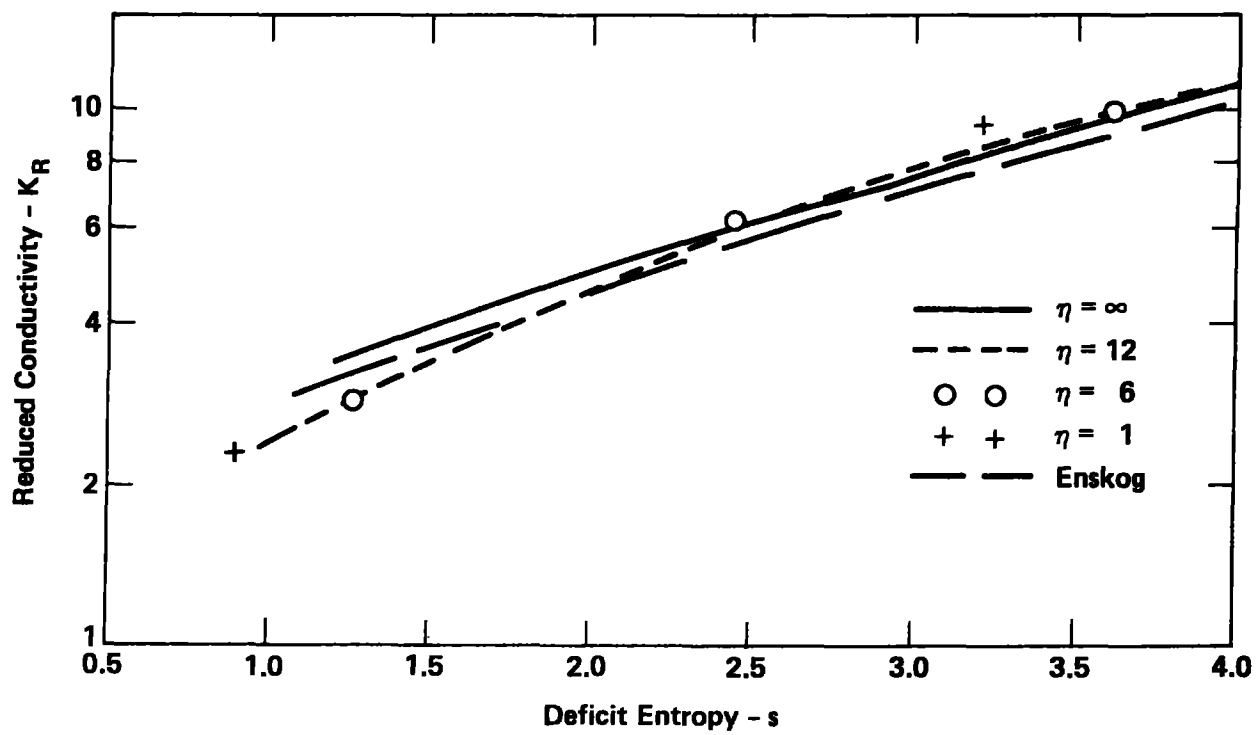


FIG. 1 Conductivity vs. entropy for 108 particle system with inverse-n pair potentials.

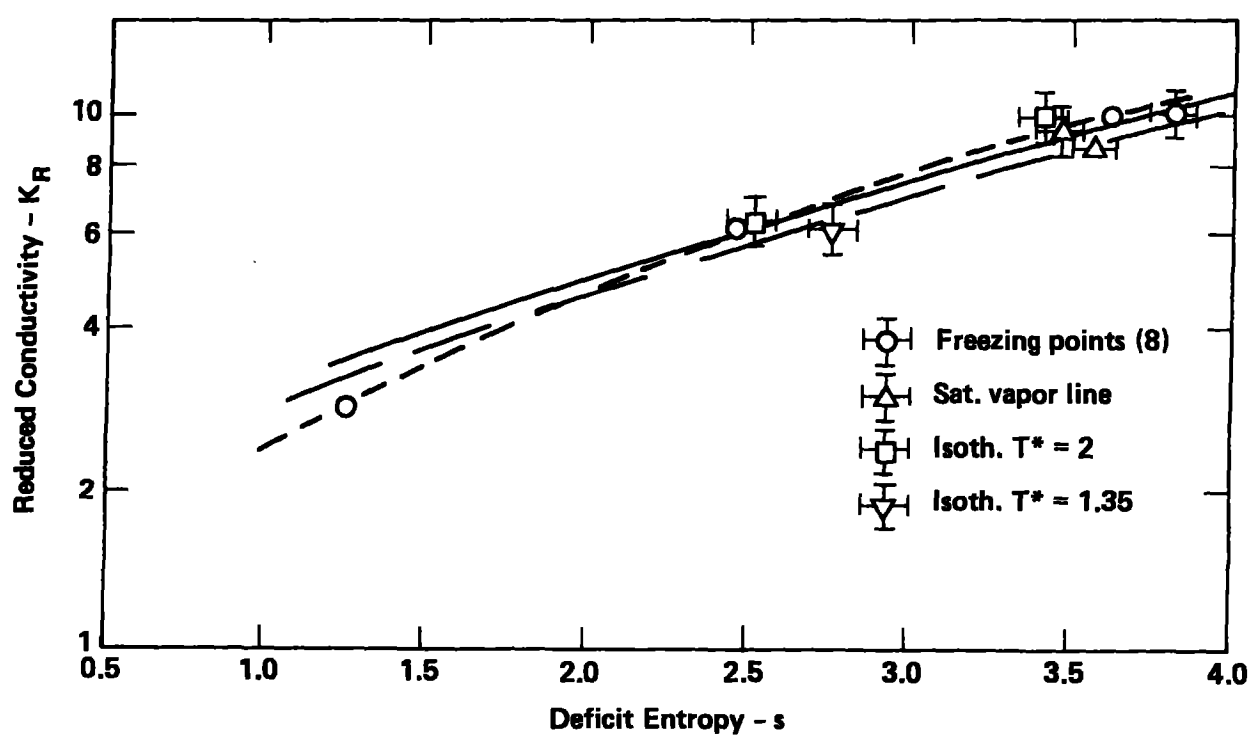


FIG. 2 Conductivity vs. entropy for the Lennard-Jones potential along various thermodynamic paths. Figure 1 results are also shown for comparison.

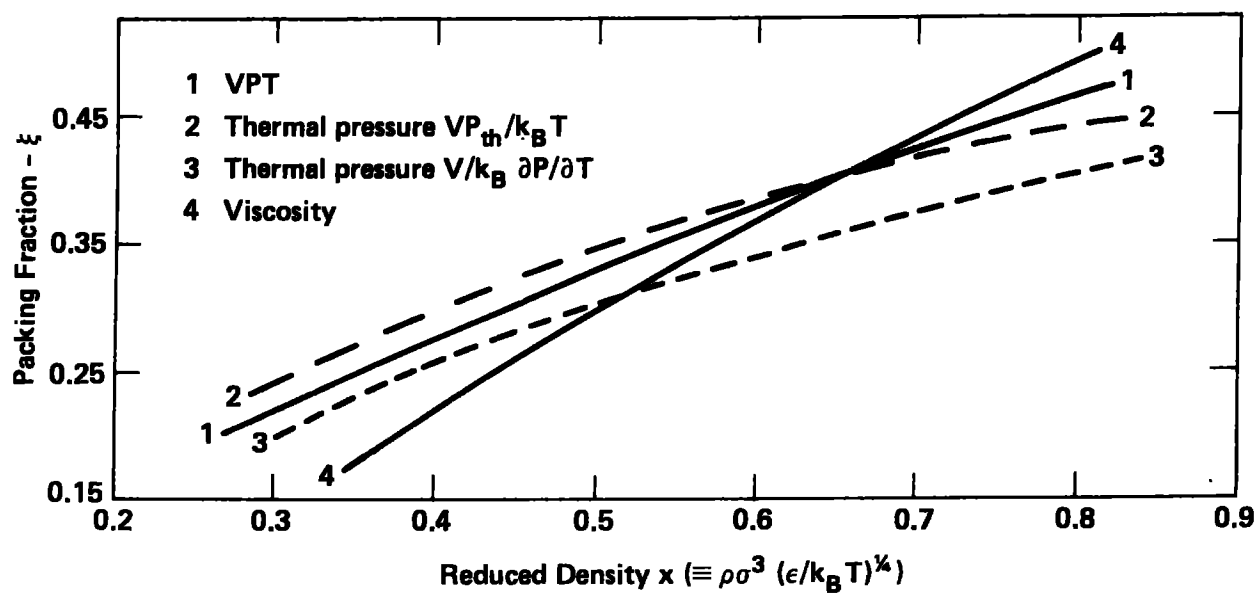


FIG. 3 Comparison of different effective hard-sphere packing fractions for the soft-sphere system ($n = 12$).

HIGH TEMPERATURE THEORY

INTERDIFFUSION IN A DENSE, BINARY IONIC MIXTURE

D. B. Boercker

- Two theoretical predictions of the interdiffusion coefficient in a binary ionic mixtures are compared. It is found that they can differ by about a factor of two in regions of practical interest where weak-coupling theories break down.

The rate at which two, initially separated, ionized materials will mix together may be estimated from the interdiffusion coefficient D for the two materials. Like most transport coefficients, the interdiffusion coefficient can be related to an integral of a time correlation function,¹

$$D = \frac{1}{3NS_{cc}} \int_0^{\infty} dt C(t) \quad (1)$$

$$C(t) = \langle (c_2 \vec{j}_1(0) - c_1 \vec{j}_2(0)) \cdot (c_2 \vec{j}_1(t) - c_1 \vec{j}_2(t)) \rangle_0, \quad (2)$$

where $N = N_1 + N_2$ is the total number of particles and $c_\alpha = N_\alpha/N$ is the concentration of species α . The total current of species α at time t is designated by

$$\vec{j}_\alpha(t) = \sum_{l=1}^{N_\alpha} \vec{v}_\alpha(l, t)$$

and S_{cc} is the hydrodynamic limit of the concentration correlation function:

$$S_{cc} = c_1 c_2 (c_2 S_{11}(k=0) + c_1 S_{22}(k=0) - 2 (c_1 c_2)^{1/2} S_{12}(k=0))$$

In the limit of either concentration becoming very small $S_{cc} \rightarrow c_1 c_2$.

The basic theoretical approach to evaluating Eq. (1) is to write down a kinetic equation for the time correlation function and express the diffusion coefficient in terms of a time integral of the "memory" function appearing in that equation. This has been done in a classical one-component plasma (OCP)

by Gould and Mazenko² for the self-diffusion coefficient and by Wallenborn and Baus³ for viscosity. Both groups used slightly different approximate forms for the "memory" function, and it is the application of these two theories to interdiffusion that will be compared here.

The interdiffusion coefficient can be written as

$$D^* \equiv D/a^2 \omega_p = \frac{c_1 c_2}{S_{cc}} \left(\frac{\pi}{3}\right)^{1/2} \frac{1}{Z_1^2 Z_2^2 \Gamma_0^{5/2} \Lambda} \left(\frac{m_1 + m_2}{2(c_1 Z_1^2 m_2 + c_2 Z_2^2 m_1)}\right)^{1/2}, \quad (3)$$

where $4\pi a^3/3 = 1/(n_1 + n_2)$, $\omega_p^2 = \omega_1^2 + \omega_2^2$, and $\Gamma_0 = e^2/ak_B T$. For low concentrations of species 2 this becomes

$$D^* = \left(\frac{\pi}{3}\right)^{1/2} \frac{1}{Z_1^3 Z_2^2 \Gamma_0^{5/2} \Lambda} \left(\frac{m_1 + m_2}{2m_2}\right)^{1/2},$$

or in units of cm^2/sec one obtains (for $c_2 \rightarrow 0$)

$$D = \frac{.0338 r_s^{1/2}}{Z_1^2 Z_2^2 \mu^{1/2} \Gamma_0^{5/2} \Lambda}, \quad (4)$$

where $r_s = a/\text{Bohr radius}$, μ is the "reduced atomic weight" of the two species and Λ is a generalization of the Coulomb logarithm. The extension of the Wallenborn-Baus theory to two components has been made in Refs. 4 and 5. The result is that Λ may be written as

$$\Lambda_{WB} = - \frac{k_B T}{4\pi Z_1 Z_2 e^2} \left(\frac{k_B T}{2\pi m_{12}}\right)^{1/2} \frac{1}{2\pi n_1 n_2} \int_0^\infty dk k^2 c_{12}(k) \int_{-\infty}^\infty d\omega [S_{11}(k, \omega) S_{22}(k, \omega) - S_{12}(k, \omega) S_{21}(k, \omega)] \quad (5)$$

The corresponding Gould-Mazenko result is

$$\Lambda_{GM} = \left(\frac{k_B T}{4\pi Z_1 Z_2 e^2}\right)^2 \left(\frac{k_B T}{2\pi m_{12}}\right)^{1/2} \frac{1}{2\pi n_1 n_2} \int_0^\infty dk k^4 c_{12}^2(k) \int_{-\infty}^\infty d\omega [S_{11}(k, \omega) S_{22}(k, \omega) - S_{12}(k, \omega) S_{21}(k, \omega)] \quad (6)$$

In Eqs. (5) and (6), the $c_{\alpha\beta}(k)$'s are the Fourier transforms of the direct correlation functions for a binary mixture and the $S_{\alpha\beta}(k, \omega)$'s are the dynamic structure factors.¹

In the weak-coupling limit, both Eq. (5) and Eq. (6) reduce to the result one would obtain from a Balescu-Guernsey-Lenard collision kernel, but they improve upon BGL by being valid for all Γ and having no large q divergence.^{2,3} Nevertheless, they differ in the way they treat the short-time behavior of the memory function from which they were obtained.^{2,3} Wallenborn and Baus retain the correct short-term behavior, Gould and Mazenko do not. This difference shows up as an extra power of $k^2 c_{12}$ inside the integral in Eq. (6).

Completing the analysis requires approximations to the structure factors. As is shown in Ref. (4b), the Vlasov equation, appropriately generalized to strong coupling, gives

$$S_{11}(k, \omega) S_{22}(k, \omega) - S_{12}(k, \omega) S_{21}(k, \omega) = \frac{2\pi n_1 n_2}{k^2} \frac{\sqrt{m_1 m_2}}{k_B T} \exp[-\omega^2(m_1 + m_2)/2k_B T k^2] |\epsilon(k, \omega)|^{-2}$$

$$\epsilon(k, \omega) = 1 - n_1 c_{11}(k) \chi_1(k, \omega) - n_2 c_{22}(k) \chi_2(k, \omega) + (c_{11}(k) c_{22}(k) - c_{12}^2(k)) \chi_1(k, \omega) \chi_2(k, \omega),$$

where $\chi_\alpha(k, \omega)$ is the usual ideal gas response function for species α . Substituting these into Eqs. (5) and (6) yields

$$\Lambda_{WB} \rightarrow - \frac{1}{3(c_1 c_2)^{1/2}} \int_0^\infty dq \, q \, S_{12}(q) \, (q) / (S_{11} S_{22} - S_{12}^2) \quad (7)$$

$$\Lambda_{GM} \rightarrow \left(\frac{1}{3\Gamma}\right)^2 \frac{1}{c_1 c_2} \int_0^\infty dq \, q^3 \, S_{12}^2(q) / (S_{11} S_{22} - S_{12}^2)^2, \quad (8)$$

where

$$S_{12}(q) = \frac{2}{\sqrt{\pi}} \int_0^\infty dy \, e^{-y^2} |\epsilon(k, kv_m y)|^{-2}$$

and

(9)

$$(m_1 + m_2) v_m^2 = 2 k_B T \quad .$$

I have numerically evaluated Eqs. (4)-(9) using the solutions to the two-component HNC equations for binary ionic mixtures of Be in Si and Si in Sr. In each case the concentration of the lighter element was taken to be $c_2 = .001$ to simulate the initial stages of mixing. The results are summarized in Tables I and II. The figures in parentheses represent the Wallenborn-Baus results.

At the points investigated, the two theories differ by factors of about 1.5-2, with the Gould-Margenko result always the larger. At present the author is unaware of any experimental or simulation data with which to compare the theories to determine which gives the better results. However, the self-diffusion coefficient for the OCP has been determined in molecular dynamics (MD) studies by Hansen, et al.⁶ The predictions of the two theories, appropriately modified, are compared to the molecular dynamics results in Table III. This comparison appears to favor the Gould-Mazenko results.

REFERENCES

1. See, for instance, N. H. March and M. P. Tosi, Atomic Dynamics in Liquids (John Wiley and Sons, New York, 1976), Chap. 6.
2. H. Gould and G. F. Mazenko, Phys. Rev. A 15, 1274 (1977).
3. J. Wallenborn and M. Baus, Phys. Rev. A 18, 1737 (1978).
4. D. B. Boercker, Phys. Rev. A 23, 1969 (1981); D. B. Boercker, F. J. Rogers, and H. E. DeWitt, Phys. Rev. A 25, 1623 (1982).
5. M. Baus, J.-P. Hansen and L. Sjogren, Phys. Lett. 82A, 180 (1981); L. Sjogren, J.-P. Hansen, and E. L. Pollock, Phys. Rev. A 24, 1544 (1981).
6. J.-P. Hansen, E. L. Pollock and I. R. McDonald, Phys. Rev. Lett. 32, 277 (1974); J.-P. Hansen, I. R. McDonald, and E. L. Pollock, Phys. Rev. A 11, 1025 (1975).

Table I. Interdiffusion coefficient (cm^2/sec) of Be in Si.

$N_{\text{Be}}/N_{\text{Si}} = .001$	$T = 0.5 \text{ keV}$	$T = 1.0 \text{ keV}$
$r_s = 3.2$.674 (.390)	1.99 (1.25)
$r_s = 4.6$	1.41 (.852)	4.34 (2.85)

Table II. Interdiffusion coefficient (cm^2/sec) of Si in Sr.

$N_{\text{Si}}/N_{\text{Sr}} = .001$	$T = 1.0 \text{ keV}$	$T = 1.5 \text{ keV}$
$r_s = 4.5$.237 (.124)	.415 (.224)
$r_s = 6.5$.499 (.269)	.875 (.491)

Table III. Self-diffusion in an OCP.

Γ	D_s^*	
	Theory	M-D
4.0	.523 (.278)	.46
19.7	.0822 (.120)	.060

OSCILLATOR STRENGTHS CALCULATED FROM EFFECTIVE POTENTIALS

B. G. Wilson and F. J. Rogers

- Effective potentials have been used to calculate multiplet absorption oscillator strengths. Comparisons with experiments on low-Z atoms are generally good.

Density-dependent absorption oscillator strengths are an essential component of opacity calculations. A large, but nevertheless insufficient, experimental database exists for some low density atoms and ions. In addition, almost no data exists for transitions at moderate plasma density. As a result, it is necessary to construct theoretical databases for materials of interest.

Due to the many possible sources of error in opacity calculations, it is not justified to require "state-of-the-art" calculations. Instead, we wish to find a qualitatively correct, computationally efficient method for constructing the required database.

Our previous success of using spherically symmetric, structure-dependent, effective potentials¹ for calculating atomic energy levels suggests that this approach may also be applicable to oscillator strengths. Since energy levels are obtained by averaging $1/r$, while oscillator strengths are obtained by averaging r , the applicability of the effective potential remains to be verified. The effective potentials used in this work have the form:

$$rV_{ei}(r) = -2\left[\xi + \sum_{n=1}^{n^*} N_n e^{-\alpha_n(\xi, \nu)r}\right], \quad (1)$$

where

$$\alpha_n(\xi, \nu) = (\xi + 1) \left(a_0(\nu) + \frac{a_1(\nu)}{\xi} + \frac{a_2(\nu)}{\xi^2} \right),$$

n is the shell responsible for the screening, N_n is the number of electrons in the n th shell $\xi = Z - \nu$, ν is the number of electrons for the parent ion and n^* the quantum number of the outermost shell of the parent. As previously used, the α_n in Eq. (1) do not depend on the ℓ of the interacting electron and we continue that procedure here.

For the present we plan to limit our research to non-relativistic atoms having $Z \leq 30$, and to LS coupling. For these conditions the multiplet absorption oscillator strength is defined according to

$$f(\gamma LS \rightarrow \gamma' L' S') = \frac{2m}{3\hbar^2 e^2} \Delta E \frac{\$}{g}, \quad (2)$$

where ΔE is the transition energy from term LS of configuration γ to excited term $L'S'$ of configuration γ' , g is the degeneracy of the ground term, and $\$$ is the transition strength calculated from pure LS coupled central field wavefunctions as

$$\$ = \delta_{SS'} (2S+1) |\langle \gamma L \| \underline{D} \| \gamma' L' \rangle|^2, \quad (3)$$

where D is the many-particle dipole operator.

For the alkali elements considerable simplification occurs due to the fact that there is only one electron outside closed shells and the term energy is simply the configuration energy. We have

$$f_{nl \rightarrow n, l \pm 1} = \frac{2m}{3\hbar^2} \Delta E \frac{l_{>}}{2l+1} \left| \int_0^\infty R_{nl} R_{n, l \pm 1} r^3 dr \right|^2 \quad (4)$$

A comparison of computed f values with those published by the National Bureau of Standards² for hydrogen, lithium, and sodium are presented in Table I.

For more complex atoms, the transition-strength formula is complicated by coupling/term dependent factors. Furthermore, at present, we have only configuration energy values whilst term energies are split about this value. For these reasons we compare computed values of the multiplet transition strength $\$$ as well as the derived quantity

$$f = \frac{2m}{3\hbar^2 e^2} \langle \Delta E \rangle \frac{\$}{g}, \quad (5)$$

where $\langle \Delta E \rangle$ is the configuration average transition energy, to published values of the multiplet strength $\$$ and

$$f = \frac{2m}{3\hbar^2 e^2} \Delta E_{\text{EXP}} \frac{\$}{g}, \quad (6)$$

where ΔE_{EXP} is the experimentally observed transition energy.

Results for second row elements sodium ($Z = 11$) through chlorine ($Z = 17$) are presented in Table II. Weise² notes that the uncertainty of these experimental numbers exceeds 50% in some cases. The overall agreement between the present calculations and experiment is fairly good although occasional large differences occur.

In the future we expect to introduce λ dependence into the screening constants α_n . Due to the smallness of this correction, a relatively simple theory should be adequate. We also expect to calculate term energy splitting in the single configuration approximation. Plasma screening corrections will be obtained from modifications of Eq. (1).

REFERENCES

1. F. J. Rogers, Phys. Rev. A23, 1008 (1981).
2. W. L. Wiese, "Atomic Transition Probabilities", NSRDS-NBS 22, Vols. I, II. (1969).

Table I. Comparison with experiment for Group-I atoms.

Transition Array	f Computed	f Ref. (2)
<u>Hydrogen</u>		
1s-2p	.4144	.4162
3s-4p	.4847	.4847
<u>Lithium</u>		
3s-3p	1.174	1.23
3p-4s	.211	.223
<u>Sodium</u>		
3s-3p	.982	.982
3s-4p	.0155	.0142
3p-4s	.171	.163
3p-3d	.858	.83
3p-4d	.0994	.106
3p-5d	.0308	.0311

Table II. Comparison with experiment for Period-III atoms.

Transition Array	Multiplet	g	\$ Computed	\$ Ref. (2)	f Computed	f Ref. (2)
<u>Magnesium</u>						
3s-3s(2s)3p	1s-1p	1	22.79	17.0	1.93	1.81
3s3p-3p2	3p-3p	9	68.38	50	.645	.61
3s2-3s(2s)4p	1s-1p	1	.1178	1.5	.0174	.22
3s3p-3s(2s)4s	3p-3s	9	29.2	21.3	.147	.139
	1p-1s	3	9.73	21.0	.147	.18
<u>Aluminum</u>						
3s23p-3s23d	2p-2d	6	37.52	10.7	.635	.175
3s23p-3s24s	2p-2s	6	8.79	9.0	.115	.115
3s23p-3s24d	2p-2d	6	5.7	2.22	.117	.0437
3s23p-3s25s	2p-2s	6	.78	.73	.015	.014
3s23p-3s25d	2p-2d	6	1.96	5.6	.043	.120
<u>Silicon</u>						
3p2-3p(2p)4s	3p-3p	9	13.98	11.6	.190	.155
	1d-1p	5	7.77	6.2	.190	.131
	1s-1p	1	1.55	1.28	.190	.100
3p4s-3p(2p)4p	3p-3d	9	239.	220.	.682	.61
	3p-3p	9	144.	130.	.411	.39
	3p-3s	9	47.8	40	.136	.13
	1p-1p	3	47.8	48.	.409	.31
	1p-1d	3	79.7	72.	.682	.67
	1p-1s	3	15.9	11.	.136	.12
	3p-3d	9	1.44	2.5	.0008	.015
3p4s-3p(2p)5p	3p-3p	9	.862	3.1	.0005	.018
	3p-3s	9	.287	1.3	.002	.0078
	1p-1p	3	.287	.0038	.005	6.1e-05
	1p-1d	3	.479	1.1	.008	.019
	1p-1s	3	.0958	.77	.002	.014
	1p-1d	3	44.8	51.	.40	.48
	1p-1p	3	14.9	.018	.133	1.0e-04
3p4p-3p(2p)4d	3d-3f	15	251.	170.	.45	.32
	3d-3p	15	183.	150.	.22	.19
3p4p-3p(2p)5s	1p-1d	3	7.91	7.0	.097	.092
3p4p-3p(2p)5d	3d-3f	15	44.32	33.0	.109	.083
<u>Phosphorus</u>						
3p3-3p2(3p)4s	4s-4p	4	6.01	7.2	.255	.307
	2d-2p	10	7.52	8.9	.128	.126
	2p-2p	6	4.51	5.4	.128	.108
3p3-3p2(1d)4s	2d-2p	10	7.52	8.9	.128	.145
	2p-2d	6	2.50	3.02	.071	.071

Table II. Comparison with experiment for Period-III atoms (continued).

Transition Array	Multiplet	g	\$ Computed	\$ Ref. (2)	f Computed	f Ref. (2)
<u>Phosphorus (continued)</u>						
3p24s-3p2(3p)4p	4p-4D	12	257.	240.	.664	.57
	4p-4S	12	154.2	140.	.399	.36
	4p-4S	12	51.4	47.	.133	.13
	2p-2p	6	77.1	77.	.399	.39
3p24s-3p2(3p)5p	4p-4p	12	1.13	3.3	.006	.016
	4p-5S	12	.376	1.5	.002	.0075
	2p-2D	6	0.94	4.2	.009	.039
	2p-2p	6	0.57	3.9	.006	.037
3p24p-3p2(3p)4d	2S-2p	2	33.81	17.	.511	.30
3p24p-3p2(3p)5d	2S-2p	2	6.18	4.3	.127	.097
	4D-4F	20	51.9	27.	.106	.057
<u>Sulfur</u>						
3p4-3p3(4s)3d	3p-3D	9	18.67	7.8	.435	.18
3p4-3p3(4s)4s	3p-3S	9	5.66	6.3	.105	.12
3p4-3p3(2d)4s	3p-3D	9	7.1	4.1	.131	.094
	1D-1D	5	14.2	6.6	.473	.24
3p4-3p3(2p)4s	3p-3p	9	4.2	5.6	.0789	.15
	1D-1p	5	2.36	3.1	.0789	.13
	1S-1p	1	1.9	1.3	.3155	.22
3p4-3p3(4s)4d	3p-3D	9	6.05	1.6	.154	.041
3p4-3p3(4s)5s	3p-3S	9	.67	.65	.016	.016
3p34s-3p3(4s)4p	5S-5p	5	194.	170.	1.18	1.1
	3S-3p	3	116.	110.	1.18	1.1
3p34s-3p3(4s)5p	5S-5p	5	1.60	.57	.0189	.0074
	3S-3p	3	.961	.25	.0189	.0048
3p34p-3p3(4s)4d	5p-5D	15	85.	93.	.181	.22
	3p-3D	9	51.	16.	.181	.059
3p34p-3p3(4s)5d	5p-5D	15	27.6	30.	.0758	.090
3p34p-3p3(4s)6s	5p-5S	15	8.4	6.8	.020	.018
	3p-3S	9	5.0	4.5	.020	.018
3p34p-3p3(4s)7s	5p-5S	15	2.3	1.9	.0067	.0059
<u>Chlorine</u>						
3p5-3p4(3p)4s	2p-2p	6	5.45	3.59	.204	.135
3p5-3p4(1d)4s	2p-2D	16	3.03	2.07	.114	.088
3p44s-3p4(3p)4p	4p-4p	12	133.	110.	.382	.30
	4p-4D	12	222.	160.	.636	.48
	4p-4S	12	44.4	31.0	.127	.11
	2p-2D	6	110.	110.	.637	.58
	2p-2S	6	2.2	21.0	.127	.11
	2D-2D	10	110.0	110.0	.382	.41
3p44s-3p4(1d)4p	4p-4D	12	1.82	.91	.010	.0052
3p44s-3p4(3p)5p	4p-4S	12	.363	.32	.0020	.0019
	2p-2D	6	.908	.20	.0099	.0021
	2p-2p	6	.545	1.5	.0060	.054
	4p-4D	12	40.6	40.8	.119	.15

COMPLIANT MATERIAL RESPONSE CHARACTERIZATION

A. C. Buckingham

- Compliant material coatings are sufficiently soft and resilient to permit yielding and deformation in response to turbulent pressure fluctuations in ocean water flowing over them. Material deformation wave amplitudes, wave lengths, and wave propagation speeds are sought which will favorably interfere with these flow pressure fluctuations so as to reduce the drag of the coated hull as it moves through the water. Attention is also given to the propagation of unstable material surface motions which may so distort the flow field that the drag increases. Experimental and theoretical analyses identify both static divergence wave deformations and Kelvin-Helmholtz flutter instabilities that appear when flow speeds are appreciably larger (three to five times) than the characteristic shear wave propagation speed of the coating material. Currently finite-element computations are used to simulate these drag producing material instabilities and to illustrate how changes to the coating material properties, internal coating composition, and internal structure may be effective in preventing their occurrence.

Duncan, Waxman, and Tulin¹ summarize the results of almost three decades of theoretical studies and introduce some new results on aerodynamic (gas phase flow) and hydrodynamic (liquid phase flow) material surface instabilities that develop in relatively soft material panels, coatings and aero/hydrofoil surfaces. Briefly, if the shear modulus of the soft material surface is relatively low, say $1/10$ to $1/100$ of a unit standard atmosphere or less (such values have been measured for soft artificial rubbers such as neoprene or viscoelastic gels such as polyvinylchloride, PVC) and if the flow speed relative to the immersed surface is about 3 or more times greater than the shear wave speed of the surface material and if the material coating depth is one to several orders of magnitude larger than the fluid boundary layer; nearly stationary surface waves or traveling waves of sufficient amplitude to disrupt the flow and the pressure distribution over the coating appear. The drag increases substantially.

Specifically, almost stationary, large amplitude instability waves develop which propagate very slowly, about one to a few percent of the material shear wave speed. When the flow to shear wave speed ratio is about 4.5 or greater, families of traveling waves appear which are trains of Kelvin-Helmholtz surface instabilities. These move at about the shear wave speed, reinforcing and growing until the entire material panel is deforming almost periodically. This latter situation is called flutter, and is more important in control and lifting surface analysis than in drag reduction studies. The discussion here is, therefore, limited to the almost stationary, static divergence surface wave instabilities.

Experimental confirmation of the presence of static divergence occurring in either turbulent or unsteady laminar flow was obtained by Hansen, Hunston, Ni, Reischman and Hoyt² and by Hansen and Hunston³ for flow over a thin homogeneous layer of low modulus PVC bonded to a rigid plate in a recirculating water tunnel. Gad-El-Hak, Blackwelder, and Riley⁴ experimentally investigated an even softer PVC coating in a towing tank facility. This PVC was reported to have the lowest shear modulus yet measured, about two orders of magnitude lower than that used in the Hansen, et al. experiments.^{2,3} The Gad-El-Hak, et al. experiments include results giving a very comprehensive time history record of the spanwise propagation and growth patterns of the instability waves. These novel records were produced through use of technically advanced laser diagnostics. These observations are of considerable interest for verification of our numerical three-dimensional compliant surface response simulations and for assistance in comparing of three-dimensional vs. two-dimensional plane strain response.⁵

Computational studies have indicated at least two candidate coating materials for drag reduction that appear to merit further, more substantial analysis and characterization.⁵ Both candidate coatings blend what seems to be an appropriate mixture of compliance with elastic resilience to counter the onset of static divergence. One of the coatings uses two layers of material bonded to each other with a stiffer thinner material outer layer fixed to the thick lower (PVC) material layer. Both are bonded to a rigid substrate. The other coating uses a patterned distribution of internal void cells (rectangular passages) with width to height aspect ratio maintained at 4:1 or greater.

Supporting the cells in a soft surrounding of low modulus PVC are reinforcing stubs of harder Neoprene rubber. The current computations emphasize numerical test of the effectiveness of these two coatings. We use direct computations over a selected parameter range of flow speed and elastic shear modulus. We produce a detailed dynamic description of the visco-elastic relaxation process and influences of internally disparate inhomogeneities which cannot be fully or even partially included in the otherwise generally instructive theoretical analyses such as that of Duncan, et al.¹

To help illustrate the substantial differences that may be expected by altering flow conditions and material properties two figures from our previous studies and analysis are reproduced here. Figure 1 shows a "long" time record (7 s) of Neoprene rubber coating, 1.5 cm thick fixed to a rigid substrate with a fully developed turbulent boundary layer pressure field exciting it. The mean potential flow speed is about 0.8 m/s and the boundary layer development length is 1 meter. This is the distance of the origin of the experimental coating measured downstream from the theoretically predicted laminar to turbulent boundary layer transition point. The record is taken at a fixed position, 1/2 the distance between beginning and end of the "test" panel of Neoprene coating which has a streamwise length of 32 cm. Typical rms deformations are of the order of $.03 \mu\text{m}$ with peak values of about $\pm 0.12 \mu\text{m}$.

The much softer Gad-El-Hak⁴ PVC coating modeled response time history is illustrated over a much shorter time record (0.5 s) in Fig. 2. We show data computed at three coating panel positions at the 1/4, 1/2, and 3/4 positions, measured from the leading edge of the panel coating. The flow speed, 10 m/s, is substantially higher than that of the previous case and the shear modulus is about three orders of magnitude lower than that of the previous Neoprene test case. The bulk modulus of the PVC is about two orders of magnitude lower than that of the Neoprene rubber. The absolute rms deformations (about $150 \mu\text{m}$) are, consequently, substantially greater than that of the Neoprene in Fig. 1. Local peak values of between 400 and $600 \mu\text{m}$ absolute deflection are recorded depending on whether the record at the leading edge (1/4) or rear portion (3/4) of the panel is examined. Analysis of the spectral response results are incomplete because of the shortness of the existing time records and the partially related lack of samples for the statistics. This (10 m/s) case is

being redone with enhanced sampling rate and a change of the development length scales to increase the frequency resolution and the advection generated phase information produced by the random scalar pressure model used to excite these surfaces.⁶

In summary, a sequence of uncoupled (random pressure model excited) coating response results are being generated for two promising compliant coatings: (1) two layer coating of thin, relatively stiff but elastic Neoprene over a thicker sublayer of soft viscoelastic PVC, with Neoprene to PVC thickness ratio of 1:5; (2) thick layer of PVC (3 times the thickness of that described in (1)) with internal voids in the form of rectangular cells, each cell having a height $1/3$ the total coating depth and a width four times that height, and with hard Neoprene rubber stiffeners imbedded in the coating, reinforcing and separating the cells. The initial computations include parametric variations of flow speed and PVC moduli. Initial computations are first generated using homogeneous PVC single layer coatings for base line response comparisons. These provide information on the onset of static divergence. Subsequent computations provide data for analysis of the enhanced drag reduction response anticipated using the two promising candidate coatings.

These results also provide both physical plane and phase plane (spectral) response characteristics useful for guidance and analysis of the direct fluid/coating interactive computational simulations described elsewhere.⁷ The information generated provides spatial resolution scales for interpolation between mesh points on the fluid or solid coating side of the interface as well as time scales to help establish time interval disparities and consequent sub-cycling requirements for direct fluid/solid interactive coupling.

REFERENCES

1. Duncan, J. H., A. M. Waxman, M. P. Tulin, "The Dynamics of Waves at the Interface Between a viscoelastic Coating and a Fluid Flow", Tech. Report Flow Industries, Inc. Kent WA, submitted to Journal of Fluid Mechanics (July, 1984).
2. Hansen, R. J., D. L. Hunston, C. C. Ni, M. M. Reischman, and J. W. Hoyt, "Hydrodynamic Drag and Surface deformations Generated by Liquid Flows over Flexible Surfaces", in Viscous Flow Drag Reduction, Progress in Aeronautics and Astronautics, Vol. 72, AIAA, NY (1979), pp 439-451.
3. Hansen, R. J., and D. L. Hunston, "Fluid Property Effects on Flow Generated Waves on a Compliant Surface", Journal of Fluid Mech. 133, 161-177 (1983).
4. Gad-El-Hak, M., R. F. Blackwelder, and J. J. Riley, "On the Interaction of Compliant Coatings with Boundary Layer Flows", Journal of Fluid Mech. 140, (in press) 257-280 (1984).
5. Buckingham, A. C., Hall, M. S., and Chun, R. C., "Numerical Simulations of Compliant Material Response to Turbulent Flow", AIAA Paper 84-0537 at AIAA 22nd Aerospace Sciences Mtg (Reno, NV, January 9-12, 1984) and currently revised for publication in AIAA Journal (1984).
6. Ash, R. L., and Khorrami, M. , "Simulation of Turbulent Wall Pressure Fluctuations for Flexible Surface Response Studies", AIAA paper 83-0292 at AIAA 21st Aerospace Sciences Mtg. (Reno, NV, January 10-13, 1983).
7. Hall, M.S., And Buckingham, A.C., "Calculation of the Interaction between a Compliant Material and an Unsteady Flow", presented at the XVIth International Congress of Theoretical and Applied Mechanics (Lyngby, Denmark August 19-25, 1984). See also following report, p. 57.

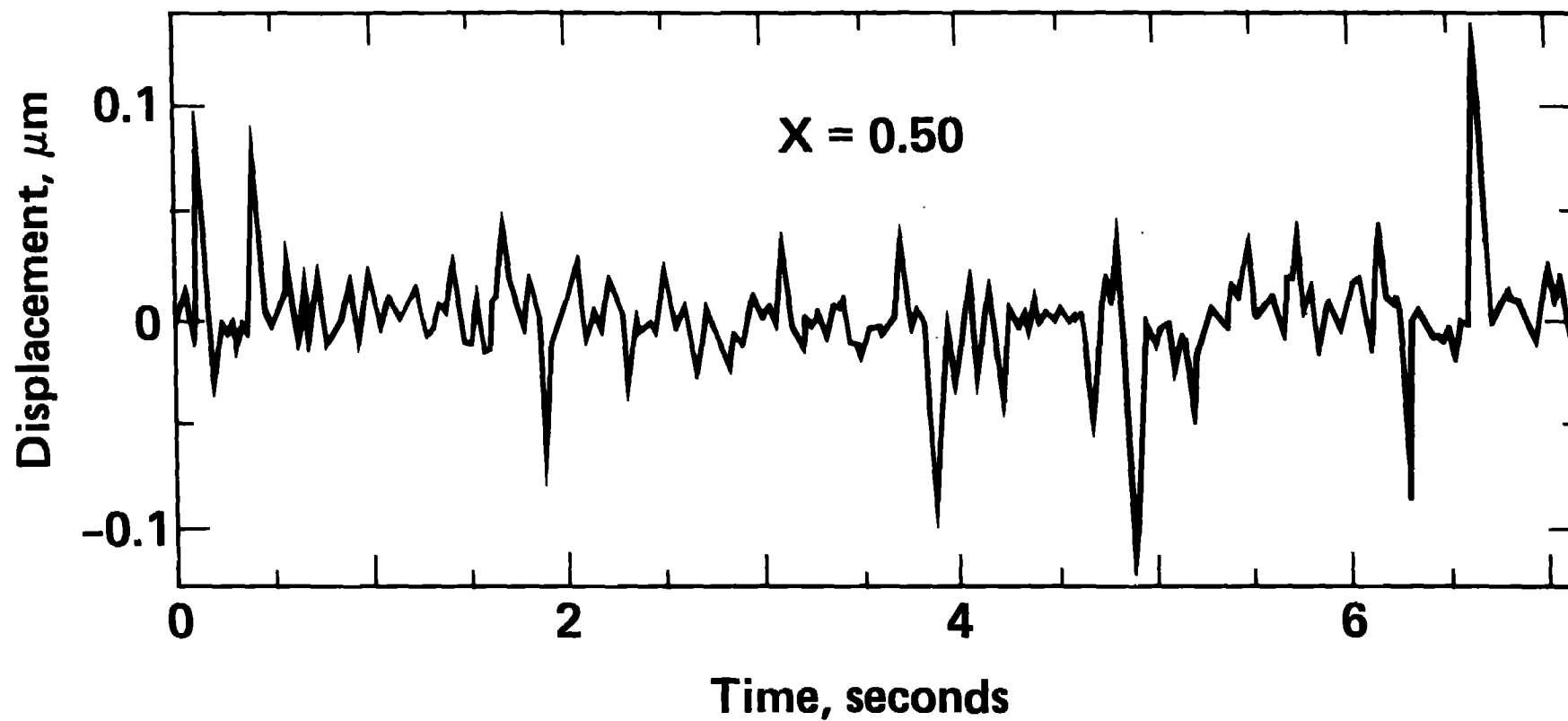


FIG. 1 Displacement time history for a compliant Neoprene rubber coating, 1.5 cm thick, subjected to a 0.8 m/s, turbulent ocean water flow. Displacements recorded at mid-position on a 32 cm long coated panel.

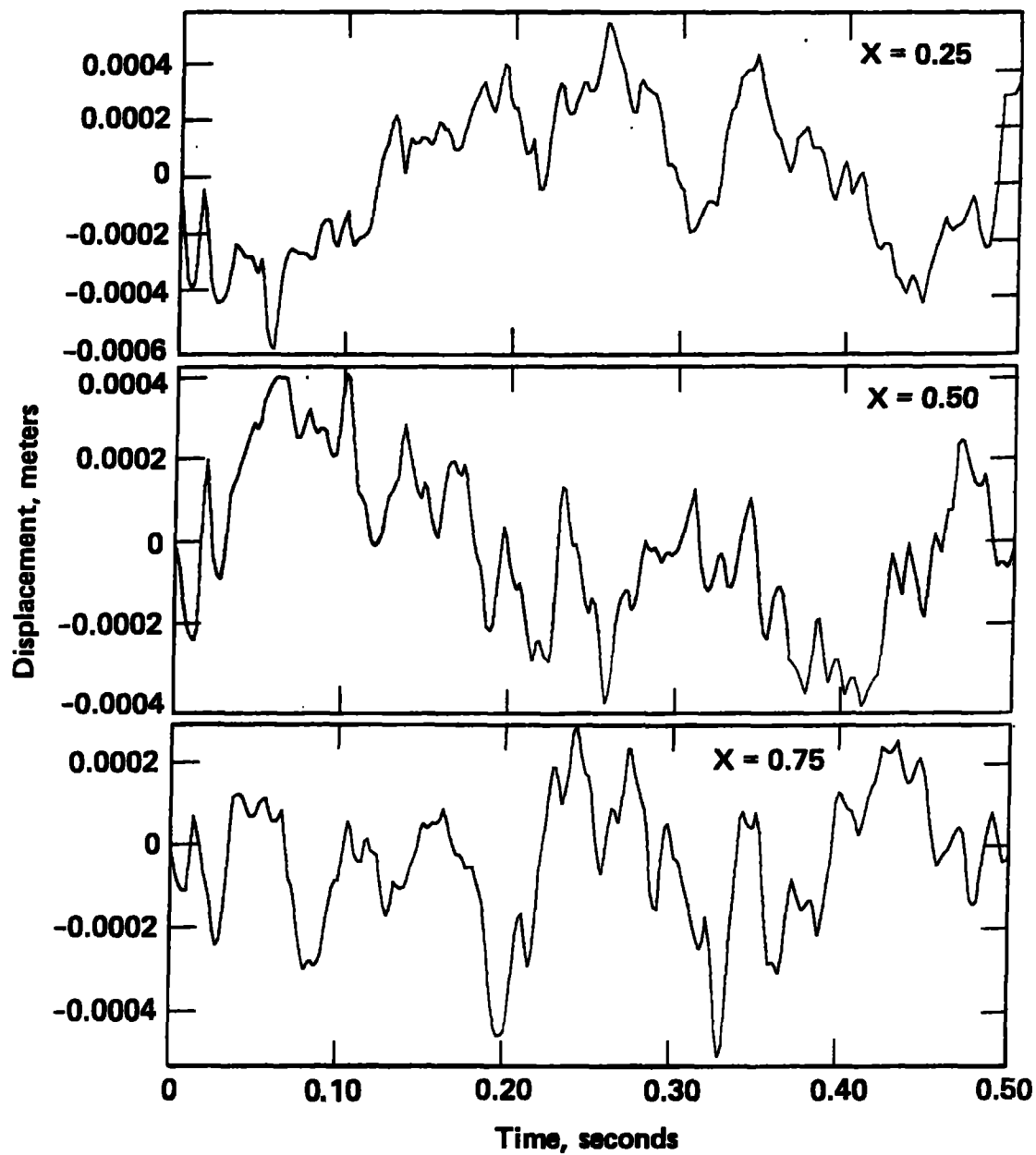


FIG. 2 Displacement time histories for compliant, very soft PVC coating modeled from the Ref. 4 experiments at 3 positions 1/4, 1/2 and 3/4 from leading edge of a 32 cm long coated panel. PVC was 4.5 cm thick and subjected to a 10 m/s turbulent ocean water flow.

NUMERICAL COUPLING OF AN UNSTABLE BOUNDARY LAYER FLOW AND A COMPLIANT SURFACE

M. S. Hall

- New pressure and viscous routines have been built into our pseudospectral fluid code that have improved the accuracy of the pressure field calculation. This new code has been coupled interactively through an exchange of boundary conditions to DYNA2D, which is used to calculate the response of a compliant material to pressures at the fluid/solid interface induced by a disturbance in the flow. This constitutes the first successful attempt to determine numerically the effect of compliant surface response on a disturbance in an unstable boundary-layer. Preliminary results for two materials are described.

The possibility of reducing the skin-friction drag on an ocean-going vessel by coating the hull with a compliant material has lead to the study of the interaction between an unsteady fluid boundary layer and a variety of visco-elastic solids. The difficulty of building layered and internally structured materials for experimental purposes has resulted in the restriction of experiments to single-layer coatings beneath turbulent boundary-layer flows.^{1,2} Difficulties in modeling complicated materials have at the same time hampered analytic studies, with the result that dispersion relations for double-layered coating materials have only recently been obtained.³ The relative ease with which the behavior of multi-layered and internally structured coatings can be studied computationally has lead to two numerical approaches: a non-interactive characterization of solid response,⁴ and the present effort, in which numerical integration of the Navier-Stokes equations has been interactively coupled through the boundary conditions to DYNA2D, the finite-element code developed by Hallquist.⁵ The difficulty associated with this coupling procedure lies both in the accurate calculation of the pressure field within the fluid domain, and in the enforcing of time-varying velocity boundary conditions on the flow field that are determined by the solid response, while maintaining sufficient accuracy in the fluid calculation to resolve structure in the boundary layer.

Numerical integration of the Navier-Stokes equations is accomplished by means of a split-operator method. The velocity is represented by a Fourier series expansion in the streamwise direction and a Chebyshev polynomial expansion normal to the fluid/solid interface. The initial condition for the flow field consists of a Blasius profile on which is superimposed an unstable solution of the Orr-Sommerfeld equation. Our initial condition and nonlinear term calculations are those developed by Metcalf and McMurray for the FLOGUN code.⁶ The nonlinear term is calculated in physical space to avoid aliasing errors and to increase computational efficiency, while the integration is done in spectral space by an explicit second-order Adams-Bashforth method. The pressure is calculated in physical space as well by a finite difference Poisson solver, to avoid oscillations that occurred in the solution due to the imposition of the velocity boundary conditions at the fluid/solid interface. The pressure is first calculated explicitly, to provide a boundary condition for the solid response that represents a physical pressure, rather than a pressure based on an intermediate velocity to which the nonlinear but not the viscous correction has been added. A freestream boundary condition is imposed at the top of the domain and periodic conditions are used in the streamwise direction. At the interface between fluid and solid, the following boundary condition provides the most stable solution:

$$\frac{\partial \pi}{\partial z} = \frac{1}{\Delta t} (\hat{W} - W) + \frac{1}{Re} \frac{\partial^2}{\partial z^2} u(t),$$

where z is the direction normal to the interface, $u = (u, w)$, π is the pressure head, and W is the component of the velocity normal to the interface, assuming zero displacement. This value is obtained from DYNA2D. Future work will include the replacing of this linearized boundary condition in which displacement is taken into account, providing analysis of the error suggests that significant improvement in the accuracy of the results would follow. Once the pressure is obtained, new values of u and w are calculated in spectral space from the u -momentum and continuity equations, respectively.

Finally, the viscous correction is done in spectral space using an implicit Spectral-Tau method, in which the equations for the coefficients of the two highest-order Chebyshev polynomials are replaced by boundary constraints. At this step, both the normal and tangential velocity boundary conditions provided by the finite element calculation are enforced.

Thus far, results have been obtained for early times (prior to breakdown of the initial disturbance) for two materials that have been used in experiments reported in the literature. These consist of a soft polyvinylchloride (PVC) used by Gad-El-Hak, et al.¹, and a firmer PVC used by Rathson.² At the transitional Reynolds', number at which we are currently doing our numerical investigations, both materials are found to deform in phase with the single-mode disturbance in such a way as to stabilize the disturbance and prevent the transfer of energy to higher modes, with the stabilization by the softer material being more rapid than that by the firmer PVC. These results are not unexpected, although experiments have shown that at higher Reynolds' numbers this tendency of the material to form "standing waves" can lead to static divergence, which in fact increases drag.¹

References

1. M. Gad-El-Hak, R. F. Balckwelder, and J. J. Riley, "On the Interaction of Compliant Coatings with Boundary Layer Flows", Journal of Fluid Mechanics **140**, 257-280 (1984) (in press).
2. A. Rathson, "Measurement of Plastisol Response to a Turbulent Boundary Layer", in Drag Reduction Symposium Proceedings, M. M. Reischman, ed. (National Academy of Science, Washington, D.C., September 13-17, 1982).
3. J. H. Duncan, "Waves in Composite Layers Bounded by Flowing Water", Tracor Hydronautics Inc., Lare1, MD Tech. Report 8111-2 (January, 1983) and personal communication (June 22, 1983).
4. A. C. Buckingham, M. S. Hall, and R. C. Chun, "Numerical Simulations of Compliant Material Response to Turbulent Flow", Lawrence Livermore National Laboratory UCRL-89400 (December, 1983).
5. J. O. Hallquist, "User's Manual for DYNA2D - An Explicit Two-Dimensional Hydrodynamic Finite Element Code With Interactive Rezoning", Lawrence Livermore National Laboratory Report UCID-18756 Rev. 2 (1984).
6. R. Metcalf, and T. McMurray, "FLOGUN Pseudo Spectral Turbulent Calculations near Compliant Walls", in Drag Reduction Symposium Proceedings, M. M. Reischman, ed. (National Academy of Sciences, Washington, D.C., September 13-17, 1982).

THREE-PARTICLE HEAT FLOW IN ONE DIMENSION VIA THE BOLTZMANN EQUATION

W. G. Hoover

- The essentials of nonequilibrium heat flow are illustrated for the simplest possible system.

The development of nonequilibrium molecular dynamics, a modification of Newtonian dynamics, has made it possible to simulate a variety of problems far from equilibrium. Steady nonequilibrium states can be characterized, numerically, or even analytically, for sufficiently simple systems. All three prototypical transport processes, diffusion, viscous flow, and heat flow have been studied.^{1,2} Diffusion and viscosity both require two bodies, with periodic boundary conditions, for numerical simulation. Heat flow requires three bodies (as indicated below). Here we describe the Boltzmann-equation approach to this problem.

Consider three particles in one dimension. The center of mass and temperature (proportional to the kinetic energy) are constrained:

$$m\dot{x}_1 + m\dot{x}_2 + m\dot{x}_3 = 0 \quad ; \quad (1)$$

$$m\dot{x}_1^2 + m\dot{x}_2^2 + m\dot{x}_3^2 = 2E \quad .$$

This system has been studied numerically, using Hooke's-law interactions³, and is stable. The velocity distribution function from (1) is:

$$f_0(p) = (\sqrt{3/2\pi}) / [(E/m) - (3p^2/4)]^{1/2} \quad . \quad (2)$$

An equation of motion, consistent with linear response theory,⁴ which will drive an isothermal heat current, is:

$$\dot{p} = \alpha[(p^2/2m) - (E/3)] - \zeta p, \quad (3)$$

where the friction coefficient ζ is chosen to ensure the constancy of $\int (p^2/2m)$:

$$\zeta = \alpha QV/2E ; QV \equiv \int (p/m)(p^2/2m) \quad (4)$$

Using the restriction (1) the heat flux can be expressed in terms of any one of the three momenta:

$$QV = (3p/2m)[(p^2/m) - E], \quad (5)$$

so that the nonequilibrium equation of motion from (3)-(5) is:

$$\dot{p} = (\alpha/12E) [-4E^2 + 15E(p^2/m) - 9(p^4/m^2)] \quad (6)$$

The relaxation-time Boltzmann equation:

$$\partial f / \partial t + \partial(\dot{f}r) / \partial r + \partial(\dot{f}p) / \partial p = (f_0 - f) / \tau, \quad (7)$$

can be solved numerically for the spatially-homogeneous steady-state distribution f , or analytically, by a series expansion in the collision time τ : $f = f_0 + \tau f_1 + \dots$. From the result,

$$f_1/f_0 = \alpha[-9(p/m) + 7(p^3/m^2)]/4, \quad (8)$$

we see that the perturbed velocity distribution resembles that found for Maxwell molecules in three dimensions, $f_1/f_0 \approx \dot{x} [(p^2/m) - 5kT]$.

We intend to investigate the extension of the calculation sketched here to two- and three-dimensional systems and into the nonlinear regime.

REFERENCES

1. D. J. Evans, W. G. Hoover, B. H. Failor, B. Moran, and A. J. C. Ladd, Phys. Rev. A 28, 1016 (1983).
2. W. G. Hoover, Physics Today 37 (January, 1984), p. 44.
3. W. G. Hoover, Physics 118A, 111 (1983).
4. D. J. Evans, Phys. Letters 91A, 457 (1982).

